[redacted]

UNCLASSIFIED

Project RAND

(U) **AERODYNAMICS, GAS DYNAMICS AND HEAT TRANSFER PROBLEMS OF A SATELLITE ROCKET**

RA-15022

February 1, 1947

UNCLASSIFIED

DOUGLAS AIRCRAFT COMPANY, INC.

[redacted]

TABLE OF CONTENTS

*This initial external distribution list includes the distribution of all related technical reports on the satellite vehicle

LIST OF FIGURES

Figure

Figure

SUMMARY

Consideration is given to the problems of a satellite rocket which involve the motion of high speed gases. These include the flow over the external surface of the rocket (drag), the flow through the rocket motor, and heat transferred to the skin of the rocket by forced convection. The skin temperatures of the satellite during its orbital motion, which depend entirely upon thermal radiation processes, are also evaluated. The discussions, although kept as general as possible, revolve around a three stage rocket employing hydrazine-liquid oxygen propellants and designed to place a 500 pound instrumentation payload on a stable orbit 350 miles above the earth. For the analyses of various features of the satellite rocket which are not covered in this report, see refs. 7, 8, 12, 18, 28 and 31.

The analysis of the drag of a satellite rocket may be considerably simplified if certain small effects are neglected, and since this allows the drag to be evaluated with an error not exceeding 10 per cent, which is sufficiently accurate for present purposes, the drag is calculated on this basis. Using these drag results, an optimum shape for the rocket is determined from the combined considerations of drag, flight mechanics, and structural weight such that the rocket has a minimum gross weight. It is found that the optimum body shape is defined by the skeleton parameter values $d/\ell_o = 0.20$ and $\ell/\ell_o = 0.80$, where d is the maximum diameter, ℓ_o is the total length, and ℓ is the length of the diverging (nose) section. However, since this result became available only during the latter part of the investigation, it was necessary to proceed on the basis of a design which resulted from an earlier study and which had the skeleton parameter values $d/\ell_o = 0.218$ and $\ell/\ell_o = 0.643$ (see Fig. 10). The drag calculations are carried out for this body shape.

To provide aerodynamic stability the first stage of the rocket is equipped with four fins having a delta planform and a modified double wedge profile. In accordance with a required lift program for the rocket, the corresponding angle of attack program is calculated, and from this the deflection of the control motor necessary to produce the required angle of attack is determined (Fig. 14). From a consideration of the rolling moments and the damping moments in pitch and yaw it is concluded that the damping moments are negligible and that the rolling moments may be adequately controlled by means of the rocket control motors. For the second stage of the rocket it was decided not to use fins to achieve aerodynamic stability, but rather to make use of the control motors to provide the necessary moments to overcome the aerodynamic instability of the body.

On the basis of rocket motor gas dynamics, calculations are carried out for the first burning period which give the average specific impulse, the ratio of specific impulse at the end and beginning of the period, and a throat area factor, which partially determines how large the throat area must be. These calculations are given for the hydrazine-oxygen and the hydrazine-fluorine propellant systems, and also for various combustion chamber pressures. The specific impulse and throat area factor are also calculated for the second and third burning periods. Owing to the extremely

small free-air pressure during the second and third burning periods, it is found that for all practical purposes the specific impulse has a constant fixed value, depending upon the combustion chamber pressure, which is the same for both periods. The same result is also true for the throat area factor. The variation of the specific impulse with height is given for the hydrazine-oxygen propellant system, this being the system chosen for the satellite rocket.

On the basis of shock wave and characteristic theory, the lift coefficient for a flat plate as a function of angle of attack is evaluated for high Mach numbers up to 10. These results are useful in calculations for winged rockets having flat plate lifting surfaces.

The investigation of the maximum skin temperature during the ascent of the rocket reveals that this is of the order of 1300°R and occurs at a height of about 40 miles. During the descent of the satellite the temperature is considerably higher, of the order of 4000°R. It seems quite likely, however, that this temperature may be considerably reduced so that melting will not occur. This could be accomplished either by using an adequate insulating layer over the skin (magnesium oxide for example) or by using wings, or perhaps by a combination of both. The skin temperatures which occur when the satellite is in its orbit vary from 400 to 960°R, neither of which represents a dangerous or objectionable extreme. The temperature difference between the earth and space sides of the satellite is about 400°R.

LIST OF SYMBOLS

A	maximum cross sectional area of rocket
A_B	base area of rocket body
A_e	exhaust area of jet
C	specific heat
C_D	drag coefficient
C_L	lift coefficient
C_M	moment coefficient about center of gravity = moment/qAd
C_p	specific heat at constant pressure
D	total drag
d	maximum diameter of rocket
d_e	diameter of jet exhaust area
F	total thrust of the rocket motors
F_c	thrust per pair of rocket control motors
F_r	resultant or net thrust exerted on rocket
g_s	gravitational conversion factor = 32.174 ft/sec^2
h	height above sea level
h	heat transfer coefficient
I	specific impulse
I_o	basic specific impulse at sea-level ambient pressure and complete expansion of the exhaust flow
J	moment of inertia
K	throat area factor
K	drag coefficient factor referring to a particular rocket
k	thermal conductivity of air
L	lift
l	mean free path of atmospheric gas particle
ℓ	length of diverging section (nose) of rocket body
ℓ_B	distance from forward end of nose to center of pressure of body lift
ℓ_R	distance from forward end of nose to control motor hinge
ℓ_T	distance from forward end of nose to center of pressure of tail surface lift
ℓ_{cg}	distance from forward end of nose to center of gravity
ℓ_o	overall length of rocket body
ℓ_x	arbitrary distance from leading edge
ℓ_2	length of diverging section of the rocket motor exhaust nozzle
log	logarithm to the base e = 2.71828

LIST OF SYMBOLS (Cont'd)

m	mass
$\dot{m}_e = \dot{m}_p$	= mass rate of propellant flow
M	Mach number
Nu	Nusselt number = h_w/k
Pr	Prandtl number = $C_p\mu/k$
p	pressure
p_c	pressure in combustion chamber
p_e	exhaust pressure
p_o	free-air (ambient) pressure
p_{oo}	standard sea-level atmospheric pressure
q	$= 1/2\rho v^2$ = dynamic pressure
Re	Reynolds number
R_u	universal gas constant
r	distance from center of earth
S	surface area
S_e	effective tail surface area
T	absolute temperature
T_c	combustion temperature
T_i	effective temperature of the boundary layer
T_o	free-air temperature at any particular altitude
T_{oo}	free-air temperature at sea level
T_T	total or stagnation temperature
T_w	skin (i.e. wall) temperature
t	time
t_b	length of burning period
V	volume
v	velocity
v_e	exhaust velocity
W	weight
W_i	total initial (gross) weight
$\dot{w}_p$	weight rate of propellant flow = $\dot{m}_p g_s$
α	angle of attack
α	absorption coefficient
α^*	effective angle of tilt
β	shock angle
Γ	ratio of temperature differences in the boundary layer
γ	ratio of specific heats

LIST OF SYMBOLS *(Cont'd)*

δ	angular deflection of control motor with respect to longitudinal axis of rocket
ϵ	emissivity
η	rocket motor efficiency factor
μ	coefficient of molecular viscosity
ν	ratio of propellant weight to gross weight
ρ	mass density
$d\sigma$	element of surface area
σ	Stefan-Boltzmann constant for radiation
ϕ	semi-vertex angle of cone
ω_o	angular speed of rotation of satellite referred to a non-rotating system of reference

AERODYNAMICS, GAS DYNAMICS AND HEAT TRANSFER PROBLEMS OF A SATELLITE ROCKET

I. AERODYNAMICS

A. DRAG

In evaluating the drag of a satellite rocket it is convenient to separate the drag into its various components, some of which are more important than others, and some of which may be neglected entirely, depending upon the accuracy required. In supersonic flow some components of drag such as that resulting from base cutoff or from interference between body and fins are not accurately known. Fortunately these effects may be neglected if great accuracy is not required.

By permitting a certain small amount of error (about 10 per cent) the drag evaluation is considerably simplified and at the same time gives results sufficiently accurate for the present investigation. Using the results of the drag evaluation, an optimum shape is determined which gives a satellite rocket of minimum gross weight.

1. The Drag Forces Exerted On a Supersonic Rocket

The drag forces on a supersonic jet propelled body such as the satellite rocket can be divided into the following parts which are listed in the order of their importance.

1. Pressure, or wave drag of the body = D_p
2. Friction drag of body and fins = D_f
3. Wave drag of the fins = D_{pf}
4. Interference drag resulting from presence of the base cutoff at the stern = D_{ib}
5. Interference drag resulting from the interaction of the jet flow and the flow over the body = D_{ij}
6. Interference drag resulting from the presence of fins on the body = D_{if}

These last three interference drag forces may be treated in the manner of small corrections and their sum will be denoted by

$$D_i = D_{ib} + D_{ij} + D_{if}. \tag{1}$$

The total drag D may then be expressed as the sum

$$D = D_p + D_f + D_{pf} + D_i . \tag{2}$$

Consider the pressure drag on the rocket body which has a base cutoff at E as shown in Fig. 1.

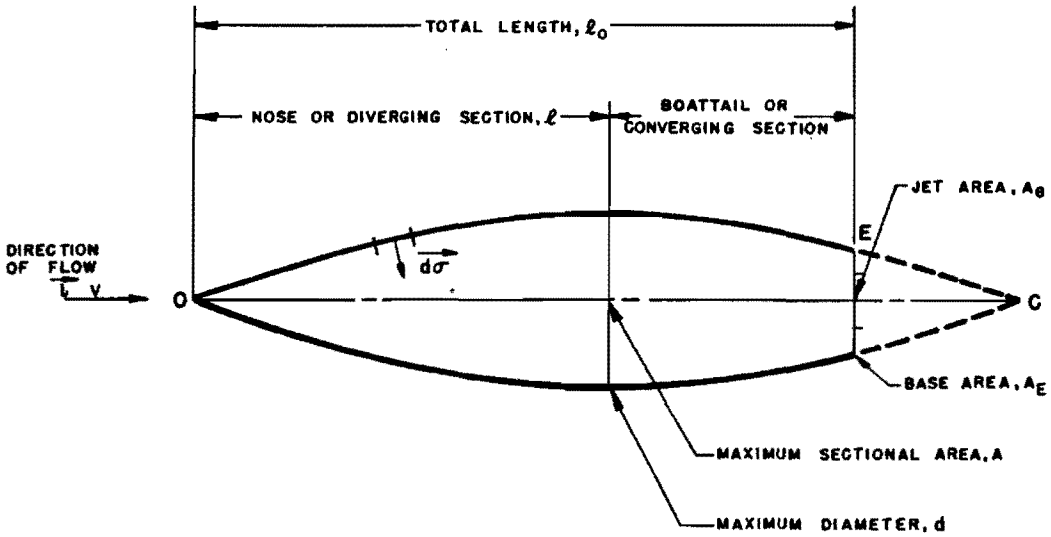

SCHEMATIC DIAGRAM OF ROCKET

FIG. 1

Letting $\vec{i}$ denote a unit vector in the direction of flow and letting $\vec{d\sigma}$ denote a vector element of surface area, positive inward, the pressure drag on the body from O to E is given by the integral

$$\oint_O^E p\, \vec{i} \cdot \vec{d\sigma} .$$

Assuming a uniform pressure p_E over the cross sectional base area A_E, and assuming further that this is equal to the free-air pressure p_o, the total pressure drag on the whole body including the base area A_E is

$$D_p = \oint_O^E p\, \vec{i} \cdot \vec{d\sigma} = \int_O^E p\, \vec{i} \cdot \vec{d\sigma} - p_o A_E = \int_O^E (p - p_o)\vec{i} \cdot \vec{d\sigma} . \tag{3}$$

This last integral on the right will be used as the definition of the pressure or wave drag, where it will be noted that the integration does not extend over the base area A_E.

The role played by this last integral in the evaluation of total drag when a jet is present will be clarified by the following illustration. Neglecting for the present, the forces D_f, D_{pf}, and D_i, if an exhaust jet fills the base area and has the same direction as $\vec{i}$, the total resultant force F_r on the body is given by

$$F_r = (\dot{m}_e v_e + p_e A_e) - \int_0^E p\, \vec{i} \cdot \vec{d\sigma}, \tag{4}$$

where $\dot{m}_e$ is the rate of mass flow issuing from the jet, v_e is the jet exhaust velocity, p_e is the exhaust pressure, and A_e (in this case $A_e = A_E$) is the exhaust area. Making use of (3), this equation becomes

$$F_r = [\dot{m}_e v_e + (p_e - p_o)A_e] - \int_0^E (p - p_o)\, \vec{i} \cdot \vec{d\sigma}. \tag{5}$$

The first term on the right in Eq. (4) is the actual internal thrust exerted on the rocket by the rocket motor. However, the first term on the right of Eq. (5), denoted by

$$F = \dot{m}_e v_e + (p_e - p_o)A_e, \tag{6}$$

is the expression commonly used for the thrust of the rocket motor. At supersonic speeds and for ideal frictionless flow, the integral occurring in Eq. (5) represents the external wave drag on the body. For ideal frictionless flow at subsonic speeds this integral vanishes, and the resultant thrust is then given by Eq. (6) which includes the drag term $p_o A_e$ resulting from the presence of the exhaust opening. Thus when the rocket thrust is defined by Eq. (6), the resultant thrust is obtained by adding the integral $\int_0^E (p - p_o)\, \vec{i} \cdot \vec{d\sigma}$ which, by Eq. (3), defines the pressure drag.

For calculating purposes it is convenient to look upon the integral

$$D_p = \int_0^E (p - p_o)\, \vec{i} \cdot \vec{d\sigma} \tag{7}$$

as the pressure drag of the body from 0 to E which would result (for idealized flow) if the body continued on to a pointed stern as shown at C, Fig. 1, and to take account of the effects of the base cutoff separately. In this case the effects of a base cutoff are reflected by the existence of a drag term D_{ib} due to the base cutoff when no jet is present, a drag D_{ij} when the jet fills the entire base area A_E, and a drag

term of the form $D_{ib} + D_{ij}$ when the jet fills only part of the base area as in the case of the satellite rocket where the jet area occupies about half of the base area. These drag effects arise, in part, because a base and a jet change the upstream flow over the boattail from that which would prevail if the body continued to C. To the drag effects induced by the presence of base and jet must also be added the skin friction drag D_f of the body and fins and the wave drag D_{pf} of the fins.

2. Approximations Used In the Drag Analysis

As far as the determination of the total drag of the satellite rocket is concerned, this will be considered satisfactory if the evaluation can be made with an *error which does not exceed 10 per cent.* On the basis of this accuracy requirement the following simplifications can be made in the analysis.

1. Since the angle of attack, α, is never to be greater than about 2° in stable flight, and actually not over 1° in the lower part of the trajectory where the aerodynamic forces are greatest, the slight increase in drag accompanying these small angles of attack will be neglected. For bodies of revolution the angle of attack may be neglected to even higher values, but for finned bodies the drag obviously increases at a greater rate with increasing α. Even when fins are present, calculations and an examination of the German A4 data show that the drag increases only about 2% for a one degree angle of attack.

2. The pressure drag on the body and fin surfaces over most of the subsonic range of speeds is negligible. At high subsonic speeds, a correction must be made which will be discussed later. At supersonic speeds the pressure drag (i.e., wave drag) on the body becomes very large. The wave drag on the 30° delta fins is still sufficiently small over the critical portion of the flight (where the highest values of the dynamic pressure q occur) that it may be neglected. Even at higher Mach numbers where the sweepback is no longer of value in reducing the drag, calculations indicate a fin wave drag of only about 3% of the total drag. Further studies of the German A4 data for bodies alone and bodies with fins indicated that the increased drag of the finned bodies could be accounted for by skin friction alone. Accordingly, the only pressure drag which will be considered at supersonic speeds is that of the rocket body alone.

3. The friction drag is included in the total drag for both body and fins at all velocities, and is calculated according to flat plate theory treating the total exposed body and fin surface as an equivalent flat plate. The error introduced by the flat plate assumption has been investigated by Göthert[1] with the results shown in Fig. 2. These results indicate that the effect on friction drag of three-dimensional flow pressure gradients is negligible for the values of d/ℓ_o applicable to the satellite rocket, (i.e., $0.1 \leq d/\ell_o \leq 0.3$) where d is the maximum diameter of the rocket and ℓ_o is the total length. The curves of Fig. 2 include a correction to the friction drag at high subsonic velocities necessitated by the effect of non-zero pressure drag due to the presence of compressibility effects. This is the correction mentioned in item 2 above.

For references see page 59

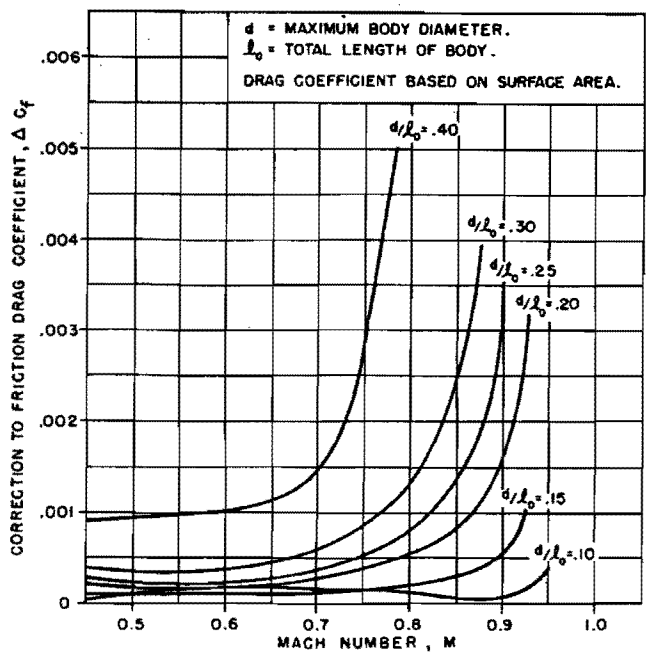

CORRECTION TO THE SUBSONIC FRICTION DRAG COEFFICIENT TO OBTAIN TOTAL SUBSONIC DRAG COEFFICIENT. AFTER GÖTHERT

FIG. 2

4. The body interference drag corrections resulting from the effects of the base, the jet, and the fins are all negligible within the 10 per cent allowable limit of error. This is justified by the following remarks. In the subsonic range, experimental tests on bodies extending to *C* (Fig. 1) show a negligible difference in the drag value as compared with bodies with bases, if the base point, *E*, is not more than half way from *C* to the maximum thickness position. In the supersonic range, however, the base pressure is considerably different from the free stream pressure so that the base drag is not zero. However calculations show that because of the small size of the base area unfilled by the jet, neglecting the base drag leaves the accuracy within the specified limits. Justification for the neglect of the fin-body interference drag was found as the result of a study based on German A4 drag data[2] for bodies with and without fins. It was found that when the friction of the fins alone was added to the friction of the body alone, the resulting value was the same as the measured friction drag of the body plus fins, thus indicating a negligible fin-body interference drag. In the subsonic range, the jet causes a reduction in pressure on the boattail section thereby causing an increase in drag while in the supersonic the jet causes an increase in boattail pressure, hence a decrease in drag. However, since very little is known concerning this effect and since the jet producing it occupies only about half of the base area, it is believed that this jet effect is quite small, and it will be neglected in both the subsonic and the supersonic range.

In summarizing these simplifications, it can be said that the total subsonic drag on the rocket consists of the friction drag of body and fins plus certain high subsonic corrections (Göthert). The total supersonic drag of the rocket consists of the friction drag on body and fins plus wave drag on the body alone. In accordance with these simplifications the total drag may be written

$$D = D_p + D_f. \tag{8}$$

3. Methods Employed In Evaluating the Drag

The wave drag, which is calculated on the basis that the gas dynamical laws are valid throughout the part of the trajectory where it is important, is discussed by separating the drag D_p into two parts, one part due to the diverging section and another part due to the boattail or converging section. The diverging section of the rocket is the part extending from the front end back to the maximum diameter; the boattail or converging section is the part extending from the maximum diameter to the stern, (see Fig. 1). The maximum diameter of the diverging section is denoted by d, and the length of the diverging section will be represented by ℓ.

From an examination of the literature on the supersonic drag of cone-shaped bodies it is found that for 'reasonable' shapes having the same value of d/ℓ the drag does not differ much, and in view of the degree of accuracy specified in the drag determination, such bodies may be considered as having the same drag. In fact the drag of a Karman-Moore ogive and that of a cone having the same d/ℓ and same volume differ by about 10%. The corresponding parabolic profile has a value lying in between[3]. This difference in drag of bodies having the same general shape varies somewhat depending on what other parameters are held constant when the shape is varied. Notwithstanding the fact that the drag does not change much for a given d/ℓ, we still require the best shape for a given d/ℓ. The determination of the optimum shape for a given d/ℓ will be discussed later. Since the cone gives a conservative value (relatively large) of drag, but still within the specified limits of accuracy, and since the cone drag is better known for the larger values of d/ℓ (the error inherent in the linearized theory is greater in magnitude than the difference between cone drag and ogive drag), the drag of the diverging section of the body will be assumed to be that of an equivalent cone. Thus the drag of the diverging section is calculated from the Taylor-Maccoll theory[4] by means of the inscribed cone whose half angle ϕ is given by $\tan \phi = d/2$. We shall denote by C_{Dpn} the conical nose wave drag, as calculated by the Taylor-Maccoll theory.

The wave drag on the boattail or converging section of the body depends, among other things, on the shape of the diverging section, and it is concerning this part of the body drag that least is known. For example, no systematic theoretical investigations have been made on this subject, and the experimental data are quite sketchy. From what qualitative information is available, it appears that the following remarks may be made.

1. The supersonic boattail wave drag varies as $1/M^2$, becoming negligible above $M = 5$ (similar to the base drag). This is similar to the variation in the nose drag coefficient which also diminishes as $1/M^2$, but which does not go to zero as

does the boattail drag but essentially to 2 $\sin^2 \theta$ (for C_D based on cross section area) at sufficiently high Mach numbers. This is the value predicted by Newtonian drag in which the air on striking the surface loses the component of its momentum normal to the surface[5, 6]. The Newtonian concept also predicts the zero drag on the boattail at the higher Mach numbers.

2. At Mach numbers between 1.5 and 2, it has been found that when the boattail angle is equal to the nose angle or does not differ by more than about 20° from the nose angle, the drag appears to be calculable on the basis of an average pressure times the subtended area normal to the flow, where the average pressure is equal to the negative of the pressure on the inscribed nose cone. On this basis the magnitude of the boattail drag can be calculated according to the equation

$$C_{D_{pbt}} = \left(C_{D_{pn}}\right)_{M = 1.75} \times \frac{(1.75)^2}{M^2} \times \frac{A - A_E}{A}, \tag{9}$$

where $C_{D_{pn}}$ is the wave-drag coefficient for the nose and $C_{D_{pbt}}$ that for the boattail. A represents the maximum cross section area and A_E is the total base area including that of the jet. The nose coefficient $C_{D_{pn}}$ is defined by

$$C_{D_{pn}} = \frac{\text{wave drag of nose}}{qA}, \tag{10}$$

where $q = 1/2\ \rho v^2$ is the dynamic pressure, and where the wave drag is calculated from the Taylor-Maccoll theory for the inscribed nose cone using $M = 1.75$. In passing, it must be remembered that high subsonic pressure drag effects are added as a correction term in the friction drag according to the data obtained by Göthert.

Using the equivalent flat plate method, the friction drag has been calculated for both body and fins, over the Mach number range extending from 0.2 to 0.925 and from 1.2 to 6. The effects of variation in Reynolds number is included in the calculations. The lower limit of Reynolds number and the upper limit of Mach number were determined from trajectory considerations; that is, the altitudes were determined at which the drag $g_s D/W$ on the rocket (where W is gross weight and g_s is acceleration of gravity) becomes negligible as far as flight performance is concerned; see the Flight Mechanics Report[7]. The lower Reynolds number limit corresponds to a trajectory altitude of about 300,000 feet. The atmospheric gas at heights of this order becomes so rarefied (see ref. 8 for analysis of the atmospheric density at high altitudes) that the gas dynamical laws are no longer strictly valid[9, 9a, 10]. However, as long as the Reynolds number is such as to predict laminar flow (but not low enough to give Stokesian flow), we are at least not beyond the 'slip' region. This will be true provided $Re > 100$ (see Tsien[10]), and in this case the gas dynamical laws may be used as a first approximation. The error in the drag determination resulting from this approximation is not of too great importance, since under such rarefied gas conditions the drag term $g_s D/W$ becomes relatively small; and any such inaccuracies in the drag have but negligible effect on the trajectory performance of the rocket.

The actual friction drag calculations were made from the laminar and turbulent boundary layer formulae given by Cope[11, 11a]. Cope finds, by means of a simple

theory, that the friction drag depends on Mach number as well as Reynolds number. For example, at $M = 2$ and $Re = 10^8$, the skin friction drag coefficient, C_f = friction drag/($q \times$ Surface Area), is about 75% that of its incompressible value. Although this result agrees very well with German experimental data, the entire problem of supersonic skin friction is in need of serious theoretical investigation. Curves of C_f based on equivalent flat plate surface area are plotted as a function of Re and M and shown in Fig. 3.

These calculated friction drags were further increased by 35% in accordance with the findings of Göthert[1] to account for 'manufacturing roughness'. The friction drag coefficient D_{Df} based on the maximum cross sectional area A is evaluated in terms of the coefficient C_f by means of the relation

$$C_{Df} = C_f \times \frac{\text{surface area}}{\text{maximum cross sectional area}} . \qquad (11)$$

It should again be pointed out that the surface area here includes that of the fins.

The drag associated with transonic flow ($0.9 \leqq M \leqq 1.2$) still remains to be considered. While the transonic phenomena are fairly well understood, the actual aerodynamic values of drag must still be obtained by experiment. Since it is impossible to produce a Mach number of 1.0 in a wind tunnel which contains a model, it becomes necessary to obtain transonic drag data from free flight tests and wing flow tests during flight. The results of such tests indicate that the maximum drag occurs in the Mach number range $1.0 \leqq M \leqq 1.2$. For bodies of small fineness ratios (length/diameter) the peak drag is nearer $M = 1.2$, and the peak is fairly flat. For thinner bodies the peak is generally at a lower Mach number and is sharper. The indications are that the maximum peak values of the drag are seldom more than 10% greater than the calculated drag for $M = 1.2$. In view of these remarks, it is considered satisfactory to use values of drag for the transonic region which are determined by interpolating over a fair curve connecting the value at $M = 0.9$ to that at $M = 1.2$. The total drag of the rocket, subsonic, transonic, and supersonic, is calculated in accordance with the methods which have been presented above.

4. The Optimum Shape For a Satellite Rocket

The previous discussion has been concerned with the methods employed in calculating the drag so that these may now be used in an investigation to determine a body shape for the satellite rocket which is the best shape from the combined considerations of aerodynamics, flight mechanics, and structure. In the Flight Mechanics study[7], the parameter ν, defined by

$$\nu = \frac{W_P}{W_i} = \frac{\text{weight of propellants consumed during a burning stage}}{\text{gross weight of the stage}} , \qquad (12)$$

is the fundamental quantity which is investigated to determine the minimum gross weight for the satellite rocket. To investigate the optimum rocket shape in a rigorous and exhaustive manner would require the following procedure:

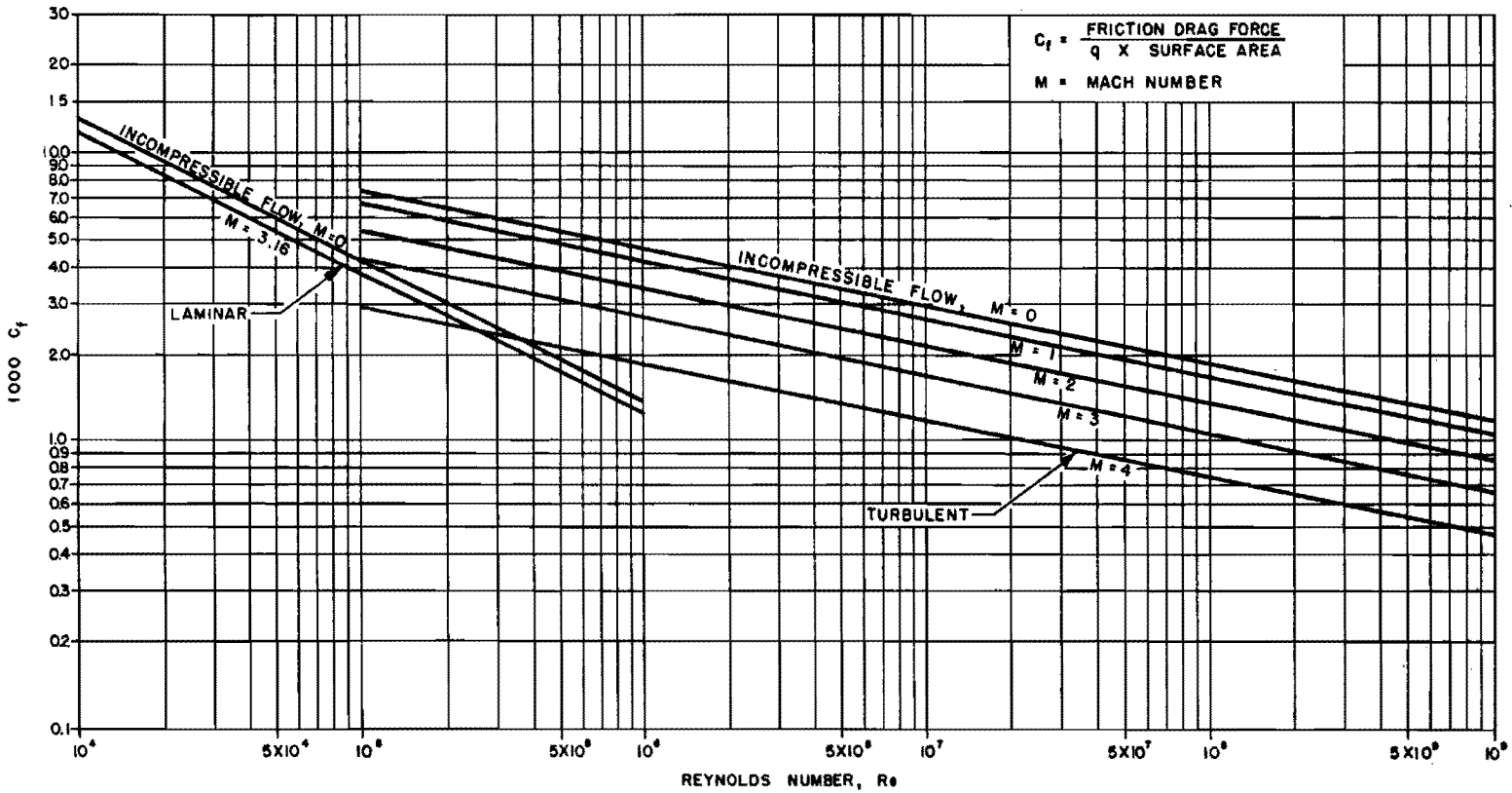

FRICTION DRAG COEFFICIENT OF A FLAT PLATE AS A FUNCTION OF REYNOLDS NUMBER AND MACH NUMBER

FIG. 3

1. Holding all trajectory shape parameters constant and for a chosen body shape, determine, according to the methods of ref. 7, the value of ν required to give the desired orbital conditions. The body shape enters the trajectory equations through a drag term $g_s D/W$, where D is total drag, W is gross weight, and g_s is the gravitational conversion factor.

2. On the basis of the value of ν thus determined and the corresponding applied load which the structure must withstand, the necessary structural weight, and therefore gross weight which the rocket must have would be determined.

3. The calculations 1 and 2 are repeated for a wide variety of possible body shapes until the shape giving the least gross weight is found.

Since this procedure would require a prohibitive amount of calculation, it is fortunate that the problem can be handled in a simpler manner as follows. Since the drag represents a small perturbation as far as the trajectory calculations are concerned, and since the best shape of body represents a small perturbation (up to 10 per cent) as far as the gross weight is concerned, it is therefore permissible to make use of the following simplified procedure in determining the optimum shape for the body; the drag of the fins will not be considered.

1. As a basis for discussion it is assumed that the gross weight is known to a zero order approximation; that is, the order of magnitude of the gross weight is known and the changes resulting from changes in shape will be reflected only as a first order change in the gross weight. In general, for any rocket stage, since the required thrust is proportional to the gross weight and since the thrust is proportional to the exhaust area, it follows that the exhaust area is proportional to the gross weight. Then, since the gross weight is assumed known to a zero order approximation, it follows that the exhaust area is known or fixed to the same order approximation. A continuation of this line of argument then shows that when the gross weight undergoes a first order change, the corresponding first order change in the exhaust area will cause a second order change in gross weight. Accordingly, the jet exhaust area A_e and the base area A_B may be considered fixed as far as the gross weight of the optimum shape is concerned.

2. Structural considerations[1,2] show that the main variables which determine the gross weight of the body are the overall shape parameters ℓ_o/d and ℓ/d, Fig. 1. When these parameters are allowed to vary subject to the restriction that the gross weight must remain constant to zero order, the volume remains constant to zero order, and the gross weight varies to a first order due to the rearrangement of material. After the best skeleton values ℓ_o/d and ℓ/d are chosen according to considerations to be described below, it is then possible to investigate the best aerodynamic lines which can be drawn upon the skeleton. Once ℓ_o/d and ℓ/d are chosen and are therefore fixed, it will be found that the possible choices of reasonable aerodynamic lines lie within such narrow limits that within this narrow range of shapes it is permissible to treat the first order values of volume and gross weight as constant. Accordingly, when the skeleton shape parameters ℓ_o/d and ℓ/d have been determined from the combined considerations of aerodynamics, flight mechanics, and structural weight, the best aerodynamic shape for least drag can be investigated on the basis of constant volume.

3. Since it is found in the trajectory calculations[7] that the maximum value of the drag term $g_s D/W$ occurs in the Mach number range $1.25 \leq M \leq 1.5$, the investigation of the optimum values for ℓ/d and ℓ_o/d will be based on $M = 1.5$. It will be assumed for this study that at other supersonic Mach numbers the percentage change in $g_s D/W$ with the body shape parameters is the same as that for $M = 1.5$. Thus when the drag integral $\mathcal{I}_{Do} = \int g_s (D/W)_o \, dt$ has been evaluated over a flight path (trajectory) for chosen values $(\ell/d)_o$ and $(\ell_o/d)_o$, the value of the integral for other values of these parameters is obtained simply by changing the value of $\mathcal{I}_{Do}$ by the same percentage that $g_s D/W$ changes at $M = 1.5$. It is assumed that changes in drag do not result in any change in the shape of the trajectory. Thus, the general drag integral $\mathcal{I}_D$ is evaluated from

$$\mathcal{I}_D = \int g_s \frac{D}{W} \, dt = \frac{C_D}{C_{Do}} \mathcal{I}_{Do} = \frac{C_D}{C_{Do}} \int g_s \left(\frac{D}{W}\right)_o \, dt, \tag{13}$$

where the subscript zero refers to quantities which are based on the best $(\ell/d)_o$ and $(\ell_o/d)_o$, the best trajectory shape, and the smallest value of ν_o known at the time. The drag coefficient C_D is evaluated by means of the formula

$$C_D = \frac{\text{total drag of body}}{q \times v_o^{2/3}}, \tag{14}$$

and is calculated for various ℓ/d and ℓ_o/d using the fixed values V_o and $d_{Eo}/V_o^{\frac{1}{3}}$, where d_{Eo} is the diameter of the base area A_{Eo}. These results are shown in Fig. 4, which gives C_D as a function of d/ℓ_o and ℓ/ℓ_o rather than of d/ℓ and d/ℓ_o. The basic drag integral $\mathcal{I}_{Do}$ is then evaluated from the relation (in this connection see Eq. (80) of ref. 7)

$$g_s \left(\frac{D}{W}\right)_o = g_s \frac{C_{Do} \, q \, V_o^{\frac{2}{3}}}{W_i \left(1 - \nu_o \frac{t}{t_b}\right)}, \tag{15}$$

where, for any particular rocket stage, W_i is the total initial (i.e., gross) weight and t_b is the length of the burning period.

4. The next step is to calculate the variation of ν as a function of ℓ/d and ℓ_o/d through the drag integral $\mathcal{I}_D = \int g_s (D/W) dt$. This is done by making use of the simplified formula (61) of ref. 7 which, for this purpose, may be written in the form

$$\log \frac{1}{1-\nu} = \left[1 + \frac{\left(\frac{C_D}{C_{Do}} - 1\right) \int g_s \left(\frac{D}{W}\right)_o dt}{\left(\sum_{j=1}^{3} g_s \bar{I}_j \log \frac{1}{1-\nu}\right)_o} \right] \log \frac{1}{1-\nu_o}. \tag{16}$$

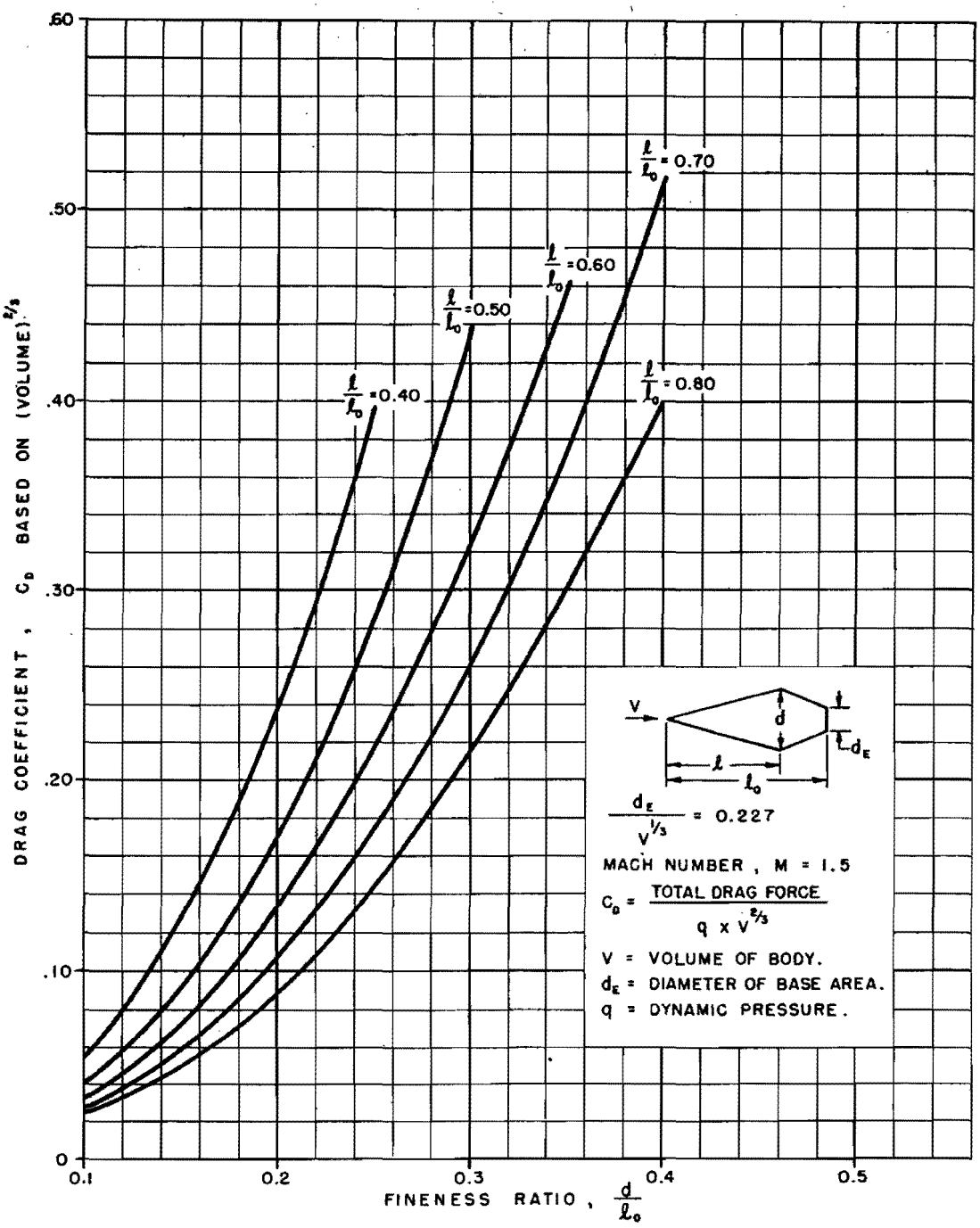

TOTAL FRICTION AND WAVE DRAG COEFFICIENT OF BODY AS A FUNCTION OF FINENESS RATIO AND RELATIVE LENGTH OF THE DIVERGING SECTION

FIG. 4

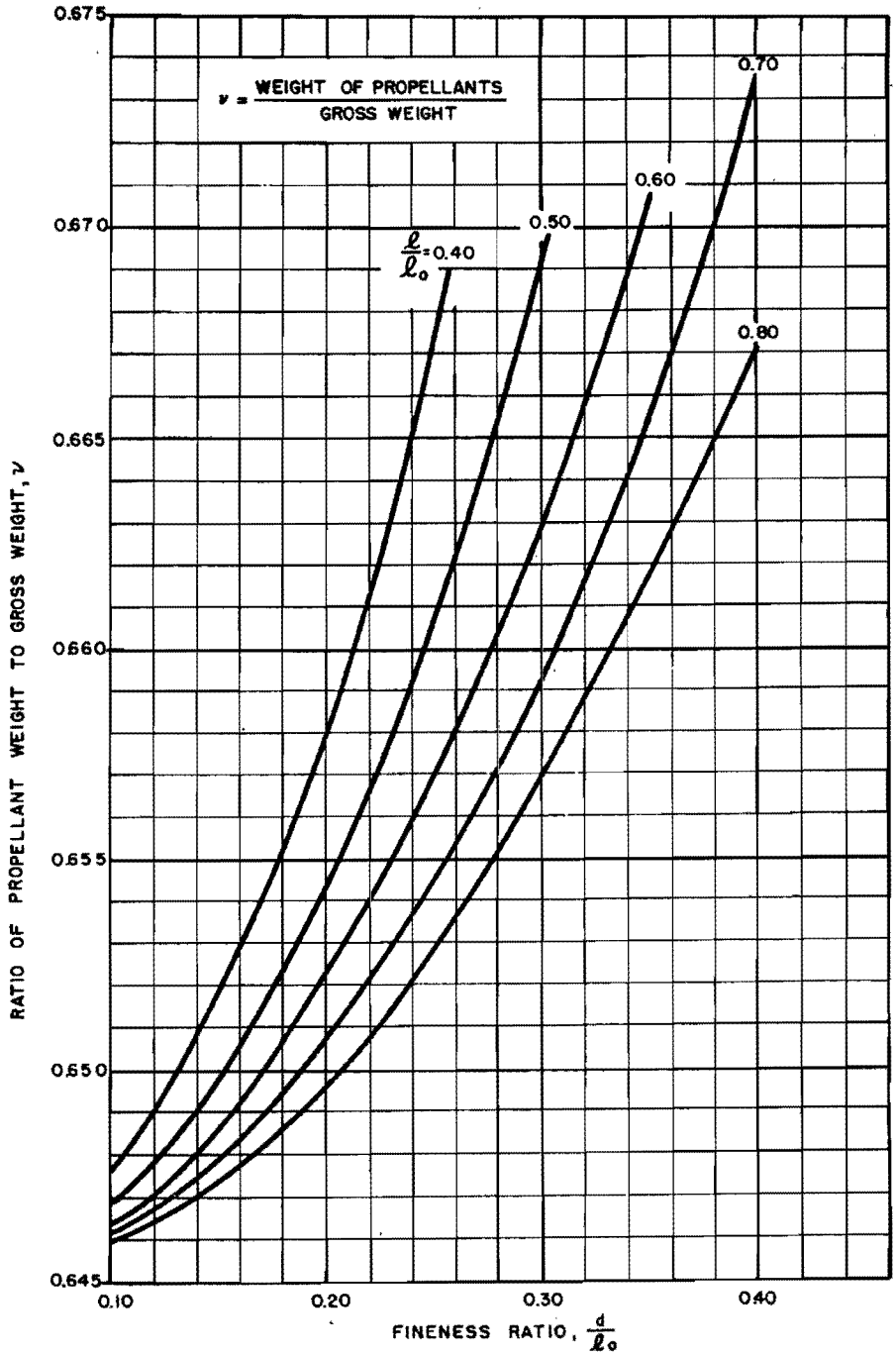

PROPELLANT-GROSS WEIGHT PARAMETER ν AS A FUNCTION OF FINENESS RATIO AND RELATIVE LENGTH OF DIVERGING SECTION

FIG. 5

The variation of ν as a function of d/ℓ_o and ℓ/ℓ_o is shown in Fig. 5. It is seen from Fig. 4 that the minimum drag coefficient is associated with large values of ℓ/ℓ_o. However, a large value of ℓ/ℓ_o requires rather severe boattail angles, which would cause poor air flow conditions over the after end of the rocket body. The optimum ℓ/ℓ_o must therefore be chosen with this in mind, and it appears that values of ℓ/ℓ_o greater than 0.80 should be avoided. These same remarks also apply to the curves for ν, Fig. 5, which show that minimum ν is associated with large values of ℓ/ℓ_o. The initial gross weight W_1 corresponding to the values of ν in Fig. 5 and calculated according to the method presented in ref. 12 is plotted in Fig. 6. On the basis of this plot it is found that the optimum values are

$$\left(\frac{\ell}{d}\right)_{opt} = 4.00 \text{ , and } \left(\frac{\ell_o}{d}\right)_{opt} = 5.00.$$

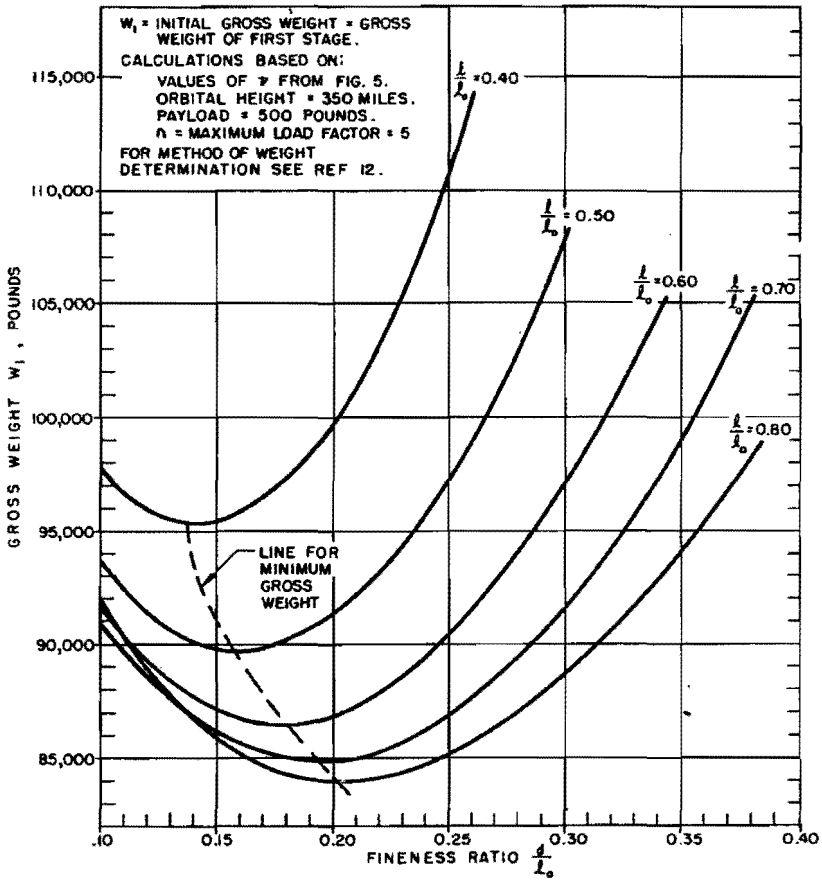

GROSS WEIGHT OF THE THREE STAGE HYDRAZINE-OXYGEN SATELLITE ROCKET AS A FUNCTION OF FINENESS RATIO AND RELATIVE LENGTH OF DIVERGING SECTION

FIG. 6

These values are based on $\left(\frac{\ell}{\ell_o}\right)_{opt} = 0.80$ and $\left(\frac{d}{\ell_o}\right)_{opt} = 0.20$.

Since time schedule limitations made it necessary to arrive at a final design for the rocket body before the study leading to Figs. 5 and 6 could be completed, the values used for ℓ/d and ℓ_o/d were those determined from a previous but less exact investigation of similar nature. It is this previously determined design which served as a basis for the values C_{D_o}, W_i, V_o $(\ell/d)_o$ and $(\ell_o/d)_o$ used in Eq. (15). This design was based on $\ell/d = 2.95$ and $\ell_o/d = 4.59$. It is seen from Fig. 6 that this results in an increase in gross weight of only about 5000 lbs.

The profile of the delta fins was determined after a consideration of both theoretical and experimental work on the subject. The final design incorporates a modified double wedge with the maximum thickness at the 50% chord position (always determined parallel to the direction of the flow). A 5% thickness ratio for the basic double wedge was decreased (from subsonic flow considerations) by fairing in (tangentially) a circular arc from the 33 1/3% chord position to the 66 2/3% chord position. This resulted in a final thickness ratio of about 4%. This small thickness ratio results in such small wave drag that only the friction drag need be considered, as explained above.

The drag coefficients used in the first and second stages of the trajectory are shown in Figs. 7 and 7A. These values are based on the maximum cross-sectional area A and are calculated over the Mach number range as described earlier. A further slight simplification was made inasmuch as it was assumed, for purposes of calculation, that the variation of C_d with Reynolds number, Re, was negligible for $M < 0.75$.

In order to use these values of C_D in the trajectory calculations, the drag term $g_s D/W$ was evaluated from the relation

$$g_s \frac{D}{W} = g_s \frac{C_D A q}{W_i \left(1 - \nu \frac{t}{t_b}\right)}, \tag{17}$$

which may be written more conveniently in the form

$$g_s \frac{D}{W} = g_s \frac{C_D A}{W_i} \times \frac{1}{2} \rho_{oo} \, (1000)^2 \times \frac{\sigma \left(\frac{v}{1000}\right)^2}{\left(1 - \nu \frac{t}{t_b}\right)}, \tag{18}$$

where W_i is the gross weight of any stage, ρ_{oo} is the standard sea level value for the atmospheric density and $\sigma \rho_{oo}$ gives the free-air density at the particular height in question (see ref. 8). Absorbing the constants in this equation into a constant K, it may be written

$$g_s \frac{D}{W} = K C_D \frac{\sigma \left(\frac{v}{1000}\right)^2}{\left(1 - \nu \frac{t}{t_b}\right)}, \tag{19}$$

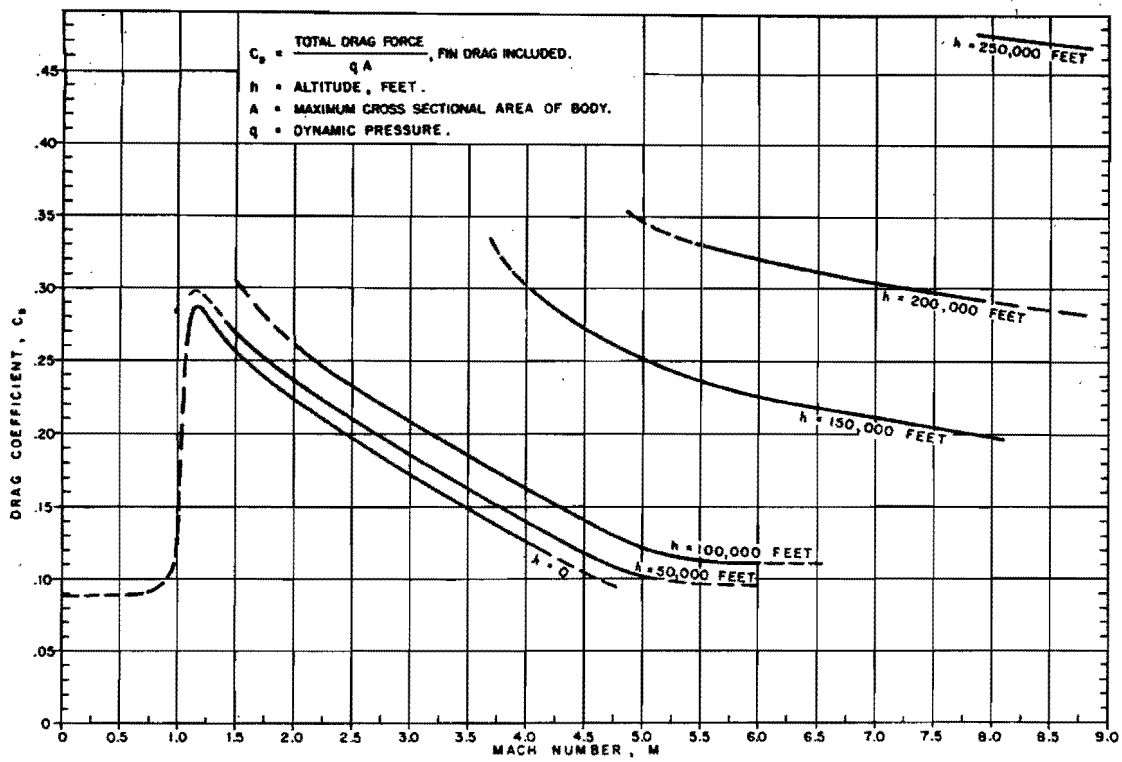

DRAG COEFFICIENT FOR THE FIRST STAGE OF THE SATELLITE ROCKET

FIG. 7

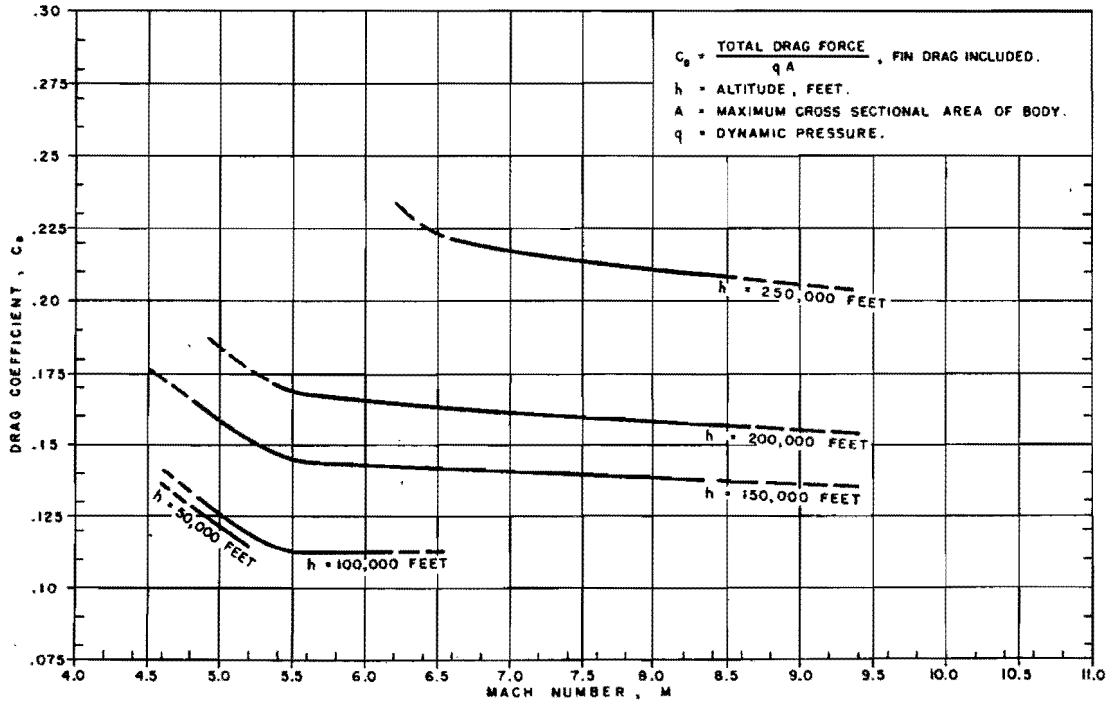

DRAG COEFFICIENT FOR THE SECOND STAGE OF THE SATELLITE ROCKET

FIG. 7A

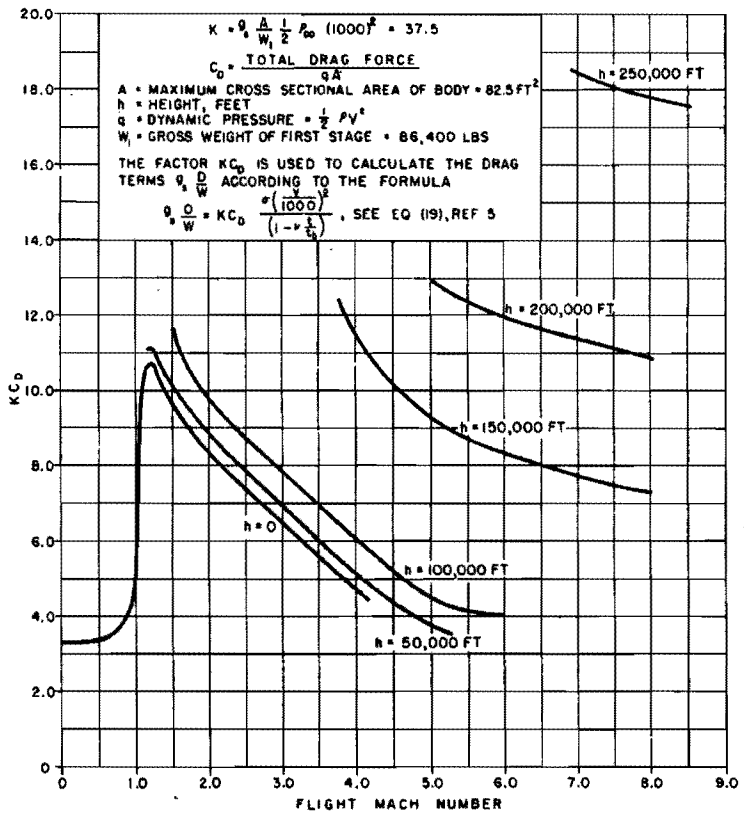

THE DRAG FACTOR KC_D AS A FUNCTION OF HEIGHT AND MACH NUMBER FOR THE FIRST STAGE OF THE THREE STAGE HYDRAZINE–OXYGEN SATELLITE ROCKET

FIG. 8

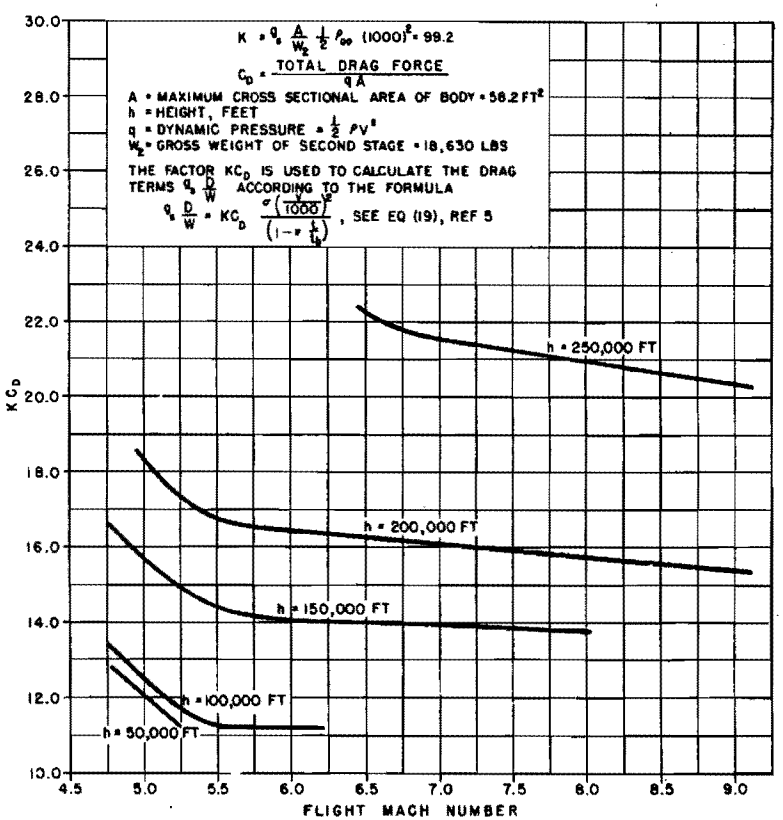

THE DRAG FACTOR KC_D AS A FUNCTION OF HEIGHT AND MACH NUMBER FOR THE SECOND STAGE OF THE THREE STAGE HYDRAZINE–OXYGEN SATELLITE ROCKET

FIG. 8A

where

$$K = g_s \frac{A}{W_i} \times \frac{1}{2} \rho_{oo} \ (1000)^2. \qquad (20)$$

The variation of KC_D with Mach number and altitude for the first and second stages is shown in Figs. 8 and 8A.

As a further aid in visualizing the function of the drag in the trajectory equations, the calculated values of D/W and the dynamic pressure q are plotted as a function of time in the trajectory for the first two burning periods (see Fig. 9).

Although the drag calculations were made on the basis of an inscribed cone extending all the way from the forward end of the nose back to the maximum diameter, it is still desirable, in order to secure better subsonic and transonic flow conditions and better supersonic stability, to adopt a better shape for the nose section, if possible, than that of a cone alone.

Of the three main body shapes given consideration — conical, parabolic, and Karman-Moore ogive — for the same ℓ/d and volume, the ogive has the least drag at low supersonic speeds. On the other hand, the cone has the least drag at high supersonic speeds, and, in addition, has a smaller body moment at low supersonic speeds. These considerations plus a consideration of the manufacturing problems involved lead to the choice of the cone for the shape of the front part of the nose and a shape lying between a parabola and a Karman-Moore ogive for the remainder of the nose and the boattail. The resulting body shape is that shown in Fig. 10.

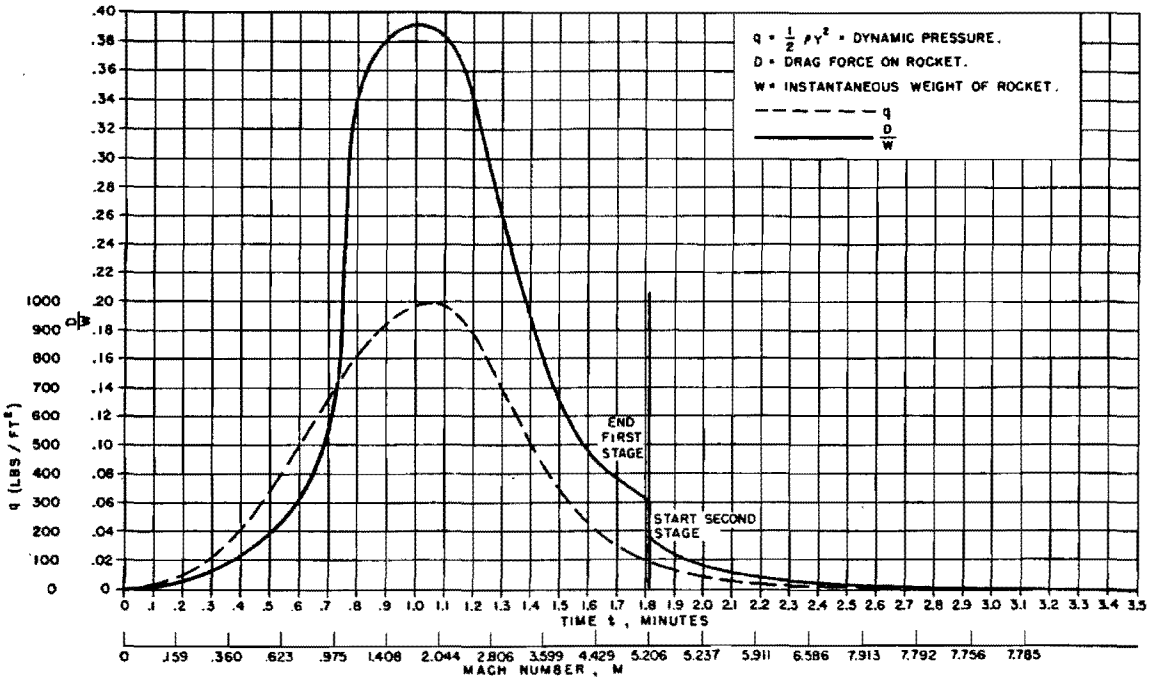

VARIATION WITH TIME AND MACH NUMBER OF THE TRAJECTORY DRAG TERM $\frac{D}{W}$ FOR THE THREE STAGE HYDRAZINE — OXYGEN SATELLITE ROCKET.

FIG. 9

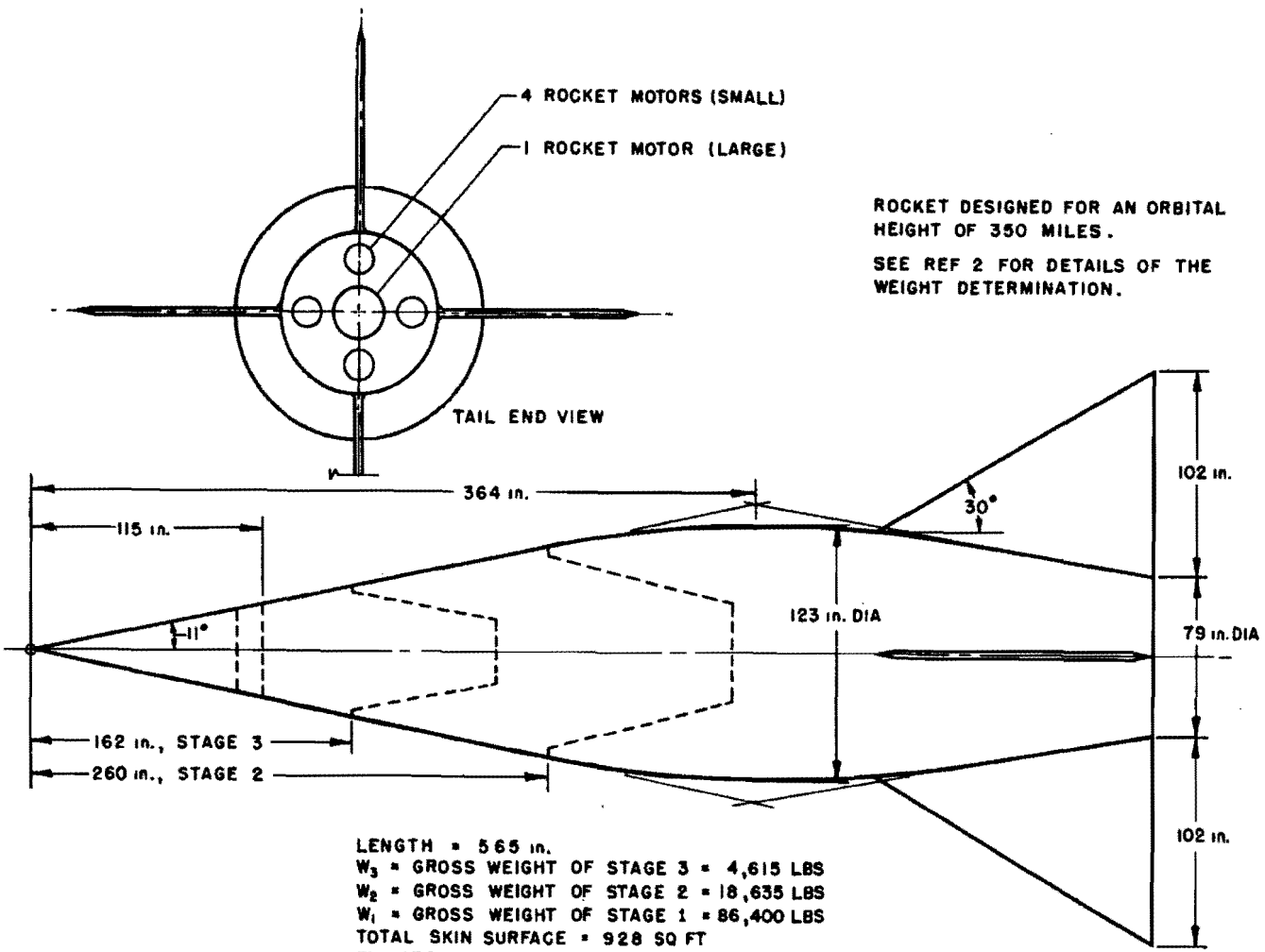

DIAGRAM OF THE THREE STAGE HYDRAZINE-OXYGEN SATELLITE ROCKET

FIG. 10

5. Rarefied Gas Dynamics (Superaerodynamics)

In making the drag calculations it was necessary to take account of the fact that at the higher altitudes where the atmosphere has the properties of a highly rarefied gas the drag coefficient can no longer be determined on the basis of the gas dynamical laws but must be calculated according to the properties of free molecule flow, Tsien[10], Sänger[9, 9a]. Thus for heights above approximately 80 miles, the atmospheric density is so low and the mean free path so large (comparable to the size of the rocket at 80 miles, see ref. 8) that the gas molecules behave as independent particles as far as the drag on the rocket is concerned. The most reasonable hypothesis to use in calculating the drag under these conditions appears to be that in which it is assumed[9, 9a, 10] that the gas particle enters the metal skin of the rocket losing all of its directed kinetic energy, comes into thermal equilibrium with the metal, and then leaves the metal skin in the manner of diffuse reflection. On this basis, the atmospheric particles upon striking the rocket lose all of their momentum; the total force on the rocket is a drag force only (no lift can be produced) having the value $\rho_o A v^2$ where ρ_o is the free-air density. This gives $C_D = 2$ as the appropriate value for the drag coefficient. This appears, at the present time at least, to represent the best value to use at high altitudes (above 80 or 90 miles) and at high supersonic speeds where the thermal velocities of the gas particles are negligible compared to the velocity of the rocket. In the lower altitude region from 60 to 80 miles it is not clear just how the drag should be calculated. In this region of the atmosphere the drag is probably determined by some combination of the gas dynamical laws and the free molecule process. For lack of anything better at present, the drag in this region is evaluated by interpolation.

The need for further research in the field of rarefied gas dynamics (also called superaerodynamics) should be emphasized. While the above ideas on free molecule flow seem quite reasonable, their verity has not actually been completely established experimentally, since they are based upon experience obtained by research on low pressure flow in pipes where the stream velocity was relatively low and in a direction parallel to the wall. Experiments should therefore be performed with very low density air moving with very high velocity and striking a surface at a finite angle. The range in densities and velocities covered should of course include the intermediate region between free molecule flow and gas dynamics.

A particularly important need for a much better knowledge of superaerodynamics in general rocket vehicle studies is that which arises in connection with the determination of lift forces in a highly rarefied gas. A knowledge of lift forces is especially important in the descent of a winged rocket. With our present knowledge the drag, at least, is known within reasonable limits; but the lift, which can greatly affect the trajectory, is not known within one or two magnitudes in the high altitude rarefied gas regions.

B. AERODYNAMICS OF STABILITY AND CONTROL

In the first burning stage of the satellite rocket trajectory large unstable aerodynamic body moments arise which must be counterbalanced by the use of a proper amount of fin area. With the lag in response of present servo-systems such large unstable aerodynamic moments could result in violent undamped oscillations of the rocket. In the second stage flight it is believed that the much smaller aerodynamic

moments can be controlled by the servo-system. It was decided therefore to provide external fins for the first stage but not for the second and third stages. The unstable aerodynamic moments in the second stage will be discussed later. The main problem to be considered here is the design of fins for the first stage. Some instability can be controlled by the servo-system, but we shall nevertheless try to design for complete stability.

Since the rocket must be stable both in pitch and yaw, and since symmetry about the roll axis is desirable, at least three fins must be used. However, it seems advisable to use four fins since this gives smaller rolling moments in cross flow than three fins and also allows the yaw and pitch controls to be separated, which permits the use of a simpler servo control system. Inasmuch as the stability requirements in pitch and yaw are practically the same and since symmetry is desirable, it was decided to use four fins of equal size and shape, spaced 90° apart. The rocket is to be controlled in a flight program of very small angles of attack, and the roll moment (due to pitch or yaw) may therefore be neglected. The damping moments in pitch, yaw, and roll will be discussed later. In accordance with the above remarks, and since the requirements on pitch stability and control are a little more stringent than that of yaw (due to the prescribed angle of attack in pitch program), the main problem reduces to the design of the two fins for pitch static stability. The resultant design will also be used for the vertical (yaw) fins.

Opposing the stability requirement (large fins desired) is the requirement of low weight, low drag, and low value of the maximum stable moment necessary to hold the prescribed tilt program (small fins desired). The last item is predicated by the desire for small rocket control moments, so that the thrust component along the flight path is kept as large as possible. Therefore the first matter that will be discussed is that of the control moment available from the rocket motors. The aerodynamic moment will be taken up later in two parts, that due to the body, and that due to the tail.

1. Control Moment

Besides a fixed rocket motor there are four movable rocket control motors, two for pitch, two for yaw, and all four for roll. The necessary control moments are provided by deflecting the control motors so that their thrusting direction is at an angle to the longitudinal axis of the rocket. The pitching moment about the center of gravity is given by

$$\text{Moment} = F_c \, (\ell_{cg} - \ell_R) \sin \delta,$$

where F_c is the thrust per pair, ℓ_{cg} is the position of the center of gravity, and ℓ_R the position of the rocket motor pivot — both measured from the forward end of the nose, and δ is the deflection of the rocket motor in degrees measured downward. The control moment coefficient is defined by

$$C_{M_R} \equiv \frac{\text{Moment}}{qAd} = \frac{F_c \sin \delta}{qA} \left(\frac{\ell_{cg}}{d} - \frac{\ell_R}{d} \right),$$

where q is the dynamic pressure, d the maximum diameter, and A the frontal area of the body ($A = \pi d^2/4$). For small angles of deflection it is convenient to define the moment coefficient by

$$C_{M_R} \equiv \delta \frac{dC_{M_R}}{d\delta} ,$$

where $dC_M/d\delta$ is the moment coefficient slope per degree. Then

$$\frac{dC_{M_R}}{d\delta} = \frac{F_c}{qA}\left(\frac{\ell_{cg}}{d} - \frac{\ell_R}{d}\right) . \qquad (21)$$

The center of gravity is practically constant during the first three-quarters of the first stage burning, moving somewhat forward during the last quarter. Redesign of fuel tanks could probably eliminate this movement. Therefore, the center of gravity is assumed constant at 359 inches from the forward end of the nose ($\ell_{cg} = 2.92\ d$). The control motor pivot is 26 inches from the base ($\ell_R = 539$ in. $= 4.38\ d$). The control motor thrust per pair is 43,800 pounds initially, increasing with altitude to 51,800 pounds at the end of the burning period. Fig. 9 gives the variation of dynamic pressure with Mach number. The control motor slope coefficient computed from Eq. (21) with $d = 123$ inches and $A = 82.5$ square feet is presented in Fig. 11 as a function of Mach number.

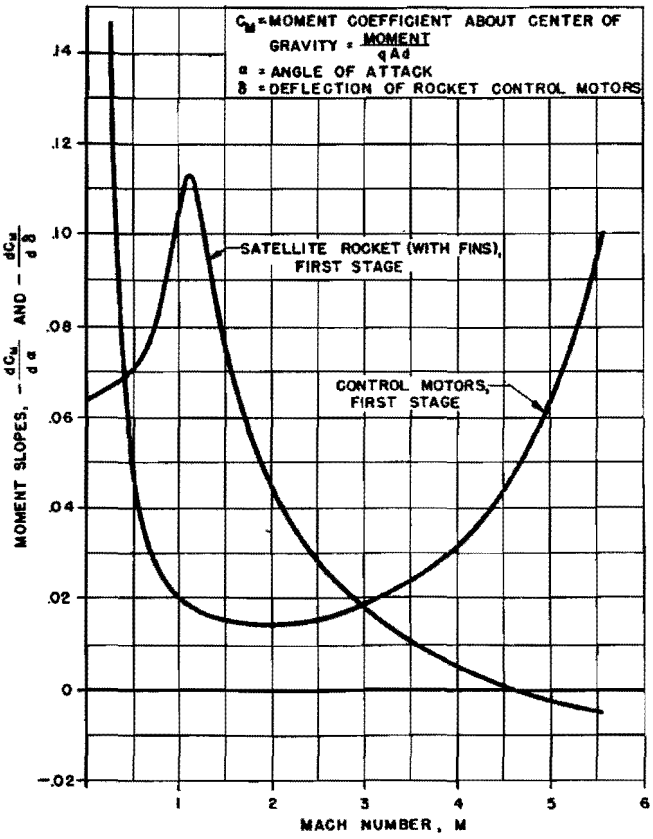

MOMENT SLOPE FOR BODY AND CONTROL MOTORS OF THE THREE STAGE HYDRAZINE – OXYGEN SATELLITE ROCKET DURING THE FIRST STAGE

FIG. 11

The maximum deflection of the rocket control motors is 15°, and it was specified that a deflection of not more than 5° should be required to hold the vehicle on course, the balance being available for corrective purposes. The actual values finally obtained will be discussed later.

2. Body Moment

The body is shown in Fig. 10. Study of available literature on body lift and center of pressure, theoretical and experimental, revealed a considerable amount of conflicting information, indicating either poor experimental work or inadequate theory. Most projectiles and missiles have a much greater length-diameter ratio and less of a boattail. The data on these more common missiles could not in a simple manner be carried over to this problem. The following analysis was therefore undertaken.

The body forces (lift and moment) were considered only for that portion of the body ahead of the fins. The body forces aft of this point can be included with the forces on the fins as described later. In subsonic or supersonic flow the presence of the tail does not essentially change the normal force distribution ahead of the maximum thickness position. In supersonic flow this is certainly true even up to the fins. Further, in subsonic flow the normal forces on the boattail are not significant except for the region of the actual tail and the body it includes. Also at very high supersonic speeds the forces are almost entirely on the front end and on the tail. This suggests that the body moments may be calculated from the lift and center of pressure on the nose section only. It is certainly not true in the low supersonic region that the lift on the portion of body between the maximum thickness and the tail is negligible, but the center of pressure moves aft if this is taken into account so that the moment changes very little. To the accuracy of our knowledge we shall calculate body moments from the nose section only.

The body nose is essentially conical. The center of pressure for a cone in supersonic flow is known to be positioned at a distance behind the nose equal to two-thirds the length of the cone. The nose section here is 364 inches so the center of pressure, ℓ_B, is taken at 241 inches = 1.97 d.

The lift coefficient is defined by

$$C_L \equiv \frac{\text{Lift}}{qA},$$

and for small angles, as before,

$$C_L = \alpha \frac{dC_L}{d\alpha},$$

where α is the angle of attack in degrees. The body moment slope is given by

$$\left(\frac{dC_M}{d\alpha}\right)_B = \left(\frac{\ell_{cg} - \ell_B}{d}\right)\left(\frac{dC_L}{d\alpha}\right)_B, \tag{22}$$

where the subscript B refers to the body. Actually the normal force N, not the lift, is desired in determining the moment. However, for small angles they are identical, and in what follows it is the normal force slope which is determined even though it is referred to as lift slope.

According to Munk the subsonic value of $(dC_M/d\alpha)_{vol}$ for the front half of a slender body of revolution is 0.015 when C_M is based on volume and when the center of gravity is located at the position of maximum thickness. Increasing this number by the factor 2.05 to give the value of $dC_M/d\alpha$ based upon Ad instead of volume results

in the value $dC_N/d\alpha = 0.0315$. At very high speeds the normal force coefficient on a cone is given by

$$C_N = \cos^2 \phi \sin 2\alpha,$$

or

$$\left(\frac{dC_N}{d\alpha}\right)_{\alpha = 0} = 2 \cos^2 \phi,$$

where ϕ is the semi-vertex angle of the cone.

The derivation is given in the Appendix. For the value $\phi = 11°$, which is used for the satellite rocket, $dC_N/d\alpha = 0.0335$ per degree. From Eq. (22) it follows that the moment slope is 0.0318.

Information for determining the body lift slope in the supersonic region is shown in Fig. 12. The upper curve was obtained by integrating the normal force distribution (as given in ref. 13) on the ogival nose of the German A4 rocket at angles of attack of 2° and 4°. Ref. 14 gives the pressure distribution on two conical-nosed projectiles tested in Italy. The integrated normal force for the nose only is shown in the figure, and Tsien's theoretical values (ref. 15) are included for comparison. Lin (ref. 16) gives theoretical results for conical-nosed projectiles having nose angles of 10° and 15° and an over-all length of $4d$. The 14° projectile of ref. 14 had an over-all length of approximately $4d$, and the measured value of $dC_L/d\alpha$ was

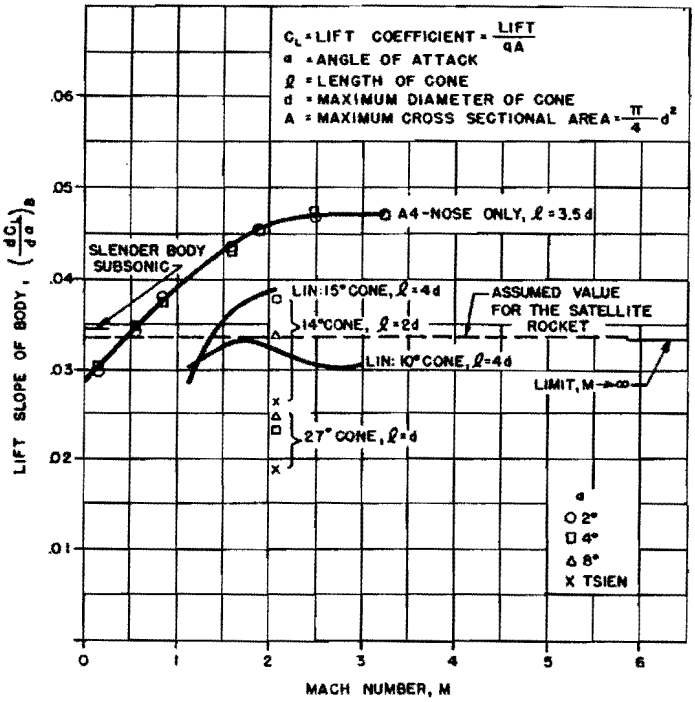

LIFT SLOPE OF VARIOUS CONE-SHAPED BODIES

FIG. 12

0.07 as compared with Lin's result of .039 for a 15° nose. It is seen that the agreement between theory and experiment is not very good.

The Lin and Tsien data for a cone show $dC_L/d\alpha$ to be .030 to .038 in the neighborhood of $M = 1$ to 2. For a cone this value falls off with increasing Mach number, but for an ogival body, as shown in Fig. 12 for the A4 nose, $dC_L/d\alpha$ goes up with increasing Mach number. Since the design here is much nearer a cone than an ogive and since there exists a serious lack of agreement between theory and experiment, it is believed that the best that can be done at this time is to use the constant value $(dC_M/d\alpha)_B = .032$ for all Mach numbers. Using this value in Eq. (22) it is found that $(dC_L/d\alpha)_B \cong 0.034$.

3. Tail Moment

The tail lift characteristics are readily obtained, but the problem of determining the effective tail* area is not a simple one. The subsonic lift was determined from unpublished wind-tunnel tests up to $M = .95$ on a delta wing with 45° semi-vertex angle (Douglas Aircraft Company, El Segundo). The value at $M = 1$ was taken from Jones' approximation, (ref. 17). The supersonic values were obtained from an unpublished compilation of available experimental information prepared by North American Aviation, Inc. The lift slope thus obtained is presented in Fig. 13.

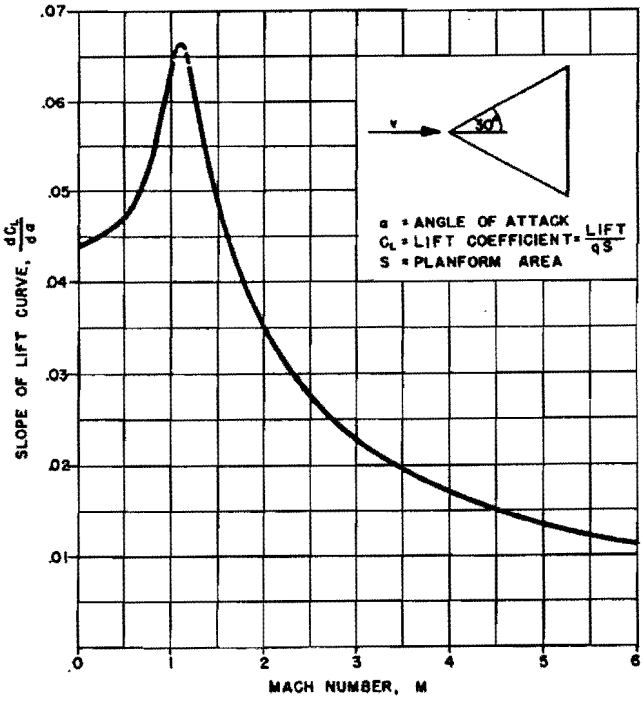

LIFT SLOPE FOR A DELTA WING

FIG. 13

* The effective tail area takes into account the lifting effect of that portion of the rocket body which separates the fins.

After some preliminary calculations the planform decided upon for the fins was one corresponding to a delta wing having a semi-vertex angle of 30° and an area of 50 square feet per fin. The delta wing planform was selected because of its favorable aerodynamic characteristics — namely the maintenance of lift, low drag, and rearward center of pressure — in the transonic and low supersonic regions.

The effective tail area was determined in the following manner. First the extreme values were determined. The maximum area is obtained by extending the delta-shaped fin clear to the center line of the body and assuming that this full area is effective in the same manner as an isolated wing. The minimum area is obtained by considering the fins alone, outside of the line extending straight back from the body junction, and placing the halves together. There are thus obtained two delta 'wings', one with 241 square feet of area, the other with but 81 square feet. The effective value is somewhere between these values and was assumed to be the mean value, 161 square feet. A delta wing of this area has a root chord of 200 inches and the center of pressure is located one-third of this length, 67 inches, from the base.

A second method is one commonly in use by the Aerodynamics Section at the Douglas Aircraft Company in which the enclosed body area is assumed to be 60 per cent effective. The area enclosed between the fins is 98 square feet. With 50 square feet of area per fin the total effective tail area is thus found to be 159 square feet.

A third method, developed by North American Aviation, Inc., gives the enclosed body area as 52 per cent effective, which corresponds to a total effective tail area of 151 square feet. The center of pressure is located 66 inches from the base.

The mean of the values obtained by these three methods is 157 square feet. The Douglas method was therefore adopted. The effective tail area was taken as 159 square feet (1.93A) with the center of pressure located 67 inches from the base, that is, ℓ_T = 498 inches = 4.05 d. The tail moment slope is then given by

$$\left(\frac{dC_M}{d\alpha}\right)_T = \left(\frac{\ell_{cg} - \ell_T}{d}\right)\left(\frac{dC_L}{d\alpha}\right)_W \frac{S_e}{A} , \qquad (23)$$

where $(dC_L/d\alpha)_W$ is the slope of the lift curve from Fig. 13 and S_e is the effective tail area.

The total aerodynamic moment slope was computed by

$$\frac{dC_M}{d\alpha} = \left(\frac{dC_M}{d\alpha}\right)_B + \left(\frac{dC_M}{d\alpha}\right)_T = .0320 + \left(\frac{dC_M}{d\alpha}\right)_T .$$

This result is presented in Fig. 11 for comparison with the control motor moment slope $dC_{M_R}/d\delta$. From Fig. 11 it will be noted that a small unstable aerodynamic moment slope is present beyond M = 4.6. It should be pointed out, however, that actually this instability may not be present because the forward movement of the center of gravity (which occurs in the present design for $M > 2$) is probably sufficient to retain the stability. In addition, because of the reduction in dynamic pressure, actual aerodynamic moments will be quite small in comparison with those of the rocket motors.

4. Control

The optimum trajectory for the satellite rocket[7] requires that after an initial period of vertical flight the rocket must be tilted in a manner to give a trajectory for which the angle of inclination θ with the horizontal has certain prescribed values. The change in θ with time is produced by the combined action of gravity and a lift force, L, normal to the trajectory. In the flight mechanics investigation[7] the total normal lift force L is specified by $F \sin \alpha^*$, where F is the total thrust and α^* is the effective angle of tilt, which reduces to the angle between the thrust vector and the tangent to the trajectory when the rocket has fixed motors and no aerodynamic lift. However, since aerodynamic lift is present and since the rocket control motors will, in general, be deflected, the actual angle of attack α is slightly different from α^*. The total lift L is defined by

$$L \equiv F \sin \alpha^* = F_{st} \sin \alpha + F_c \sin (\alpha + \delta) + L_a \tag{24}$$

where F_{st} is the thrust of the stationary motor and the yaw motors, F_c is the thrust of the control (pitch) motors, and L_a is the aerodynamic lift.

For small angles, as before, $F = F_{st} + F_c$, and

$$F\alpha^* = (F_{st} + F_c)\alpha + F_c\delta + 57.3\, L_a = F\alpha + F_c\delta + 57.3\, L_a \,. \tag{24a}$$

The aerodynamic lift is given by

$$L_a = \alpha\, q\, A \frac{dC_L}{d\alpha} \,,$$

in which

$$\frac{dC_L}{d\alpha} = \left(\frac{dC_L}{d\alpha}\right)_B + \left(\frac{dC_L}{d\alpha}\right)_W \frac{S_e}{A} \,.$$

This flight program calls for a continuous turning of the rocket about a transverse axis so that it will always be headed along the prescribed trajectory. The flight condition, therefore, is that the applied moments shall be equal to the time rate of change of the angular momentum of the rocket. This condition gives the relation

$$\text{Aerodynamic moment} + \text{control moment} = J \frac{d^2(\theta + \alpha)}{dt^2} \,, \tag{25}$$

where J is the moment of inertia of the rocket about the center of gravity. This may be written

$$57.3\, \alpha q A d \frac{dC_M}{d\alpha} + F_c\delta(\ell_{cg} - \ell_R) = J \frac{d^2(\theta + \alpha)}{dt^2} \,.$$

Letting $x = (\ell_R - \ell_{cg})/d$, this becomes

$$F_c\delta = 57.3\, \alpha q A \frac{1}{x} \frac{dC_M}{d\alpha} - \frac{J}{xd} \frac{d^2(\theta + \alpha)}{dt^2} \,. \tag{25a}$$

Substituting this expression in Eq. (24a) yields

$$F\alpha^* = F\alpha + 57.3\, \alpha qA \left(\frac{dC_L}{d\alpha} + \frac{1}{x}\frac{dC_M}{d\alpha}\right) - \frac{J}{xd}\frac{d^2(\theta + \alpha)}{dt^2},$$

which may be written in the form

$$\alpha\left(1 + 57.3\,\frac{\frac{dC_L}{d\alpha} + \frac{1}{x}\frac{dC_M}{d\alpha}}{C_F}\right) - \alpha^* = \frac{J}{Fxd}\frac{d^2(\theta + \alpha)}{dx^2}, \qquad (26)$$

where $C_F \equiv F/qA$.

Both θ and α^* are prescribed by the flight program as functions of time, and all quantities in Eq. (26) are known except α. Using the iterative process, Eq. (26) may be integrated numerically by assuming values of α at each step such as to satisfy the prescribed values of θ and α^*. Eq. (25a) is then used to calculate the required control motor deflection δ.

However, a consideration of the order of magnitude of the terms in Eq. (26) results in an important simplification inasmuch as it is found that the inertial term may be neglected, and thus the differential equation becomes simply an algebraic equation. Initially the moment of inertia is approximately equal to 150,000 slug-ft^2, decreasing to 116,000 slug-ft^2 at the end of the first burning period. The thrust increases from an initial value of 124,000 lbs to a final value of 147,000 lbs. Hence, the coefficient J/Fxd has an initial value of 0.08 and decreases to a final value of 0.04 in the first stage. The second derivative is at most of the order of 0.10 so that the right hand term is at most of the order of 0.008, a quantity negligible in comparison with a mean value of α^*. Eq. (26) may therefore be solved with sufficient accuracy by means of the relation

$$\alpha = \alpha^* \frac{1}{1 + 57.3\,\frac{\frac{dC_L}{d\alpha} + \frac{1}{x}\frac{dC_M}{d\alpha}}{C_F}}. \qquad (26a)$$

Figure 14 gives α^* the effective tilt angle as prescribed by the flight program, α the corresponding actual angle of attack, and δ the control motor deflection required to produce these values of α. These values are given for the first burning period only, since for the remaining part of the trajectory the angle of tilt α is always zero.

5. Damping Moment

The German data indicate that the damping moments in pitch do not vary much with body shape. The A4 damping moment ($\partial C_{damp}/\partial\dot{\alpha} \approx 0.9$, where $C_{damp} \equiv 24$ damping moment/$\rho V l^3 d$) was entered into the control calculations (see ref. 18) and was found at most to be one per cent of the servo applied damping moment necessary for proper control. Since this aerodynamic damping moment is negligibly small, no further investigation of this effect was necessary.

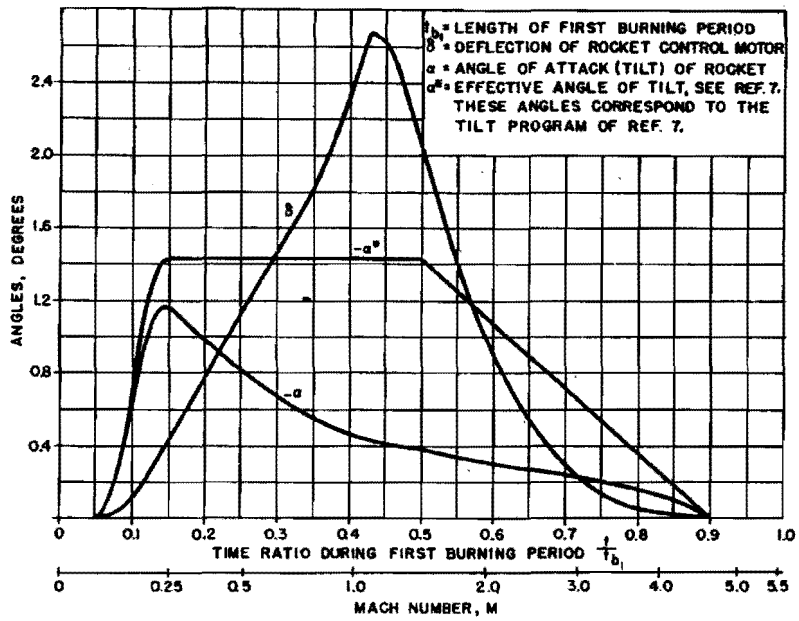

ANGLE OF ATTACK AND MOTOR DEFLECTION FOR THE THREE STAGE HYDRAZINE-OXYGEN SATELLITE ROCKET DURING THE FIRST BURNING PERIOD

FIG. 14

6. Rolling Moment

Approximate calculations of an elementary nature show that the static rolling moments, arising in the first stage from gusts or when the angle of attack is, for example, three times larger than that prescribed, are of the order of 5000 ft-lbs. Moments of this magnitude can be adequately compensated for by the rocket control motors. The damping moments in roll, like the damping moments in pitch, are negligible compared with the damping moments provided through the servo-system.

7. Stability of the Second Stage

At the start of stage 2 there will be a short interval in which the rocket will be aerodynamically unstable. The moment slope coefficient is given as before by

$$\frac{dC_M}{d\alpha} = \frac{dC_L}{d\alpha}\left(\frac{\ell_{cg} - \ell_B}{d}\right),$$

where $dC_L/d\alpha$ is taken as 0.0335 for very high Mach numbers and the center of pressure is taken as two-thirds the nose length, i.e., $\ell_B = 2/3 \times 260 = 173$ in., $\ell_{cg} = 244$ inches, $d = 101$ inches. This gives $dC_M/d\alpha = 0.0235$.

For the second stage the moment slope coefficient is referred to volume by using the multiplying factor 0.712 which gives $(dC_M/d\alpha)_{vol} = 0.0167$, nearly the same as the value at the lower Mach numbers for the first stage. Owing to the low values of q during the second stage, it is believed that the servo-system (rocket control motors) can be used to provide satisfactory control over this aerodynamic instability.

II. GAS DYNAMICS

A. ROCKET MOTOR GAS DYNAMICS AND DESIGN

The principal gas dynamical problem arising in the design of the satellite rocket is that of the proper design of the rocket motors to give the greatest possible thrust consistent with least weight and space required for the motor in each rocket stage. In general this will require a different design for each stage.

The discussion contained in this section does not present a complete story in itself but rather is intended mainly as a collection of the gas dynamical relations and information which it is necessary to have in connection with other phases of the satellite rocket investigation. No attempt will be made here to derive any of the basic gas dynamical relations, since these are well known and are adequately explained elsewhere (see refs. 19, 20 and 21 for example).

By use of Eulers' momentum theorem[22, 23] (impulse theorem), it can be shown[24] that the thrust F produced by a rocket motor is given by*

$$F = \int_{A_e} v_{ex} \frac{dm_p'}{dt} + \int_{A_e} (p_e - p_o)\, dA_e \,, \tag{27}$$

where v_{ex} = axial component of the exhaust velocity

$\frac{dm_p'}{dt}$ = element of mass of propellants flowing through the exhaust area of the nozzle per second (i.e., the rate of mass flow through an element of exhaust area)

p_e = exhaust pressure

p_o = free-air (ambient) pressure

A_e = exhaust area.

When the flow is one-dimensional so that $v_{ex} = v_e$ is the total exhaust velocity, the thrust expression becomes

$$F = v_e \frac{dm_p}{dt} + (p_e - p_o)A_e \,, \tag{28}$$

where dm_p/dt is the rate of the *total* mass flow of propellants. If further, the expansion of the exhaust flow is complete so that $p_e = p_o$, the thrust has the special value F_o where

$$F_o = v_e \frac{dm_p}{dt} \,. \tag{29}$$

* See also Eqs. (3)-(7) in Part I.

This is readily shown[25] to be the maximum thrust obtainable from a rocket motor. Although complete expansion of the exhaust flow to free-air pressure is highly desirable since it gives the maximum thrust condition, this usually requires such a long exhaust nozzle that, in order to keep the size of the nozzle within practical limits, it becomes necessary to design the nozzle for underexpansion with $p_e > p_a$.

A rocket motor consists of a combustion chamber and an exhaust nozzle as shown in Fig. 15.

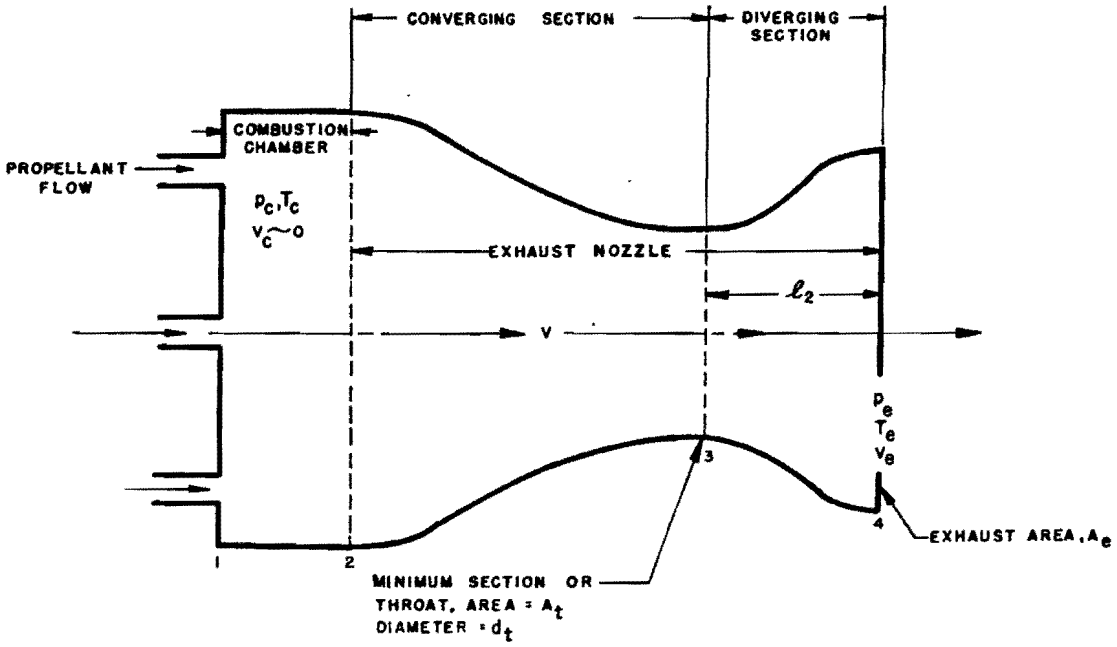

SCHEMATIC DIAGRAM OF ROCKET MOTOR

FIG. 15

The propellants flow into the motor at 1, and burn in the combustion chamber, 1 to 2, reaching the absolute temperature T_c and the pressure p_c. Assuming the combustion to be complete by the time the gases reach 2, the products of combustion flow nearly adiabatically through the exhaust nozzle 2 to 4, which has a minimum section at 3 where the local sonic velocity is reached, and an expanding portion 3 to 4 where the supersonic flow expands with decreasing pressure. When all of the burning is completed at 2 and if there is no friction or shock wave in the exhaust nozzle, the flow from 2 to 4 will be isentropic. Since the main component of the flow is in the axial direction, it is usually sufficient to treat the flow as one dimensional. Thus, on the basis of one-dimensional isentropic flow, the exhaust velocity v_e is found to be[24, 26, 27]

$$v_e = \left[2\frac{R_u}{M} T_c \left(\frac{\gamma}{\gamma - 1}\right)\left(1 - \frac{T_e}{T_c}\right)\right]^{\frac{1}{2}} = \sqrt{R_u}\sqrt{\frac{T_c}{M}} \left\{\left(\frac{2\gamma}{\gamma - 1}\right)\left[1 - \left(\frac{p_e}{p_c}\right)^{\frac{\gamma - 1}{\gamma}}\right]\right\}^{\frac{1}{2}}, \quad (30)$$

where the isentropic pressure-temperature relation has been used. R_u is the universal gas constant, M is the molecular weight of the products of combustion, $\gamma = C_p/C_v$ is the average ratio of the specific heats over the temperature range T_c to T_e, and the temperatures are expressed on the absolute scale as demanded by the equation of state $p = \rho(R_u/M)T$. The basic specific impulse I_o is defined by

$$I_o = \frac{F_o}{g_s \frac{dm_p}{dt}} = \frac{v_e}{g_s}, \tag{31}$$

where F_o is the thrust corresponding to complete expansion of one-dimensional flow to sea-level ambient pressure, Eq. (29), and g_s is the gravitational conversion constant. Thus the basic specific impulse is given in terms of the combustion chamber and exhaust conditions by the expression

$$I_o = \frac{\sqrt{R_u}}{g_s}\sqrt{\frac{T_c}{M}}\left\{\frac{2\gamma}{\gamma - 1}\left[1 - \left(\frac{p_o}{p_c}\right)^{\frac{\gamma - 1}{\gamma}}\right]\right\}^{\frac{1}{2}}. \tag{32}$$

This equation is commonly used in investigating the specific impulse of different propellants as is done in the Liquid Propellant Report[28]. The values of I_o used in this report are taken from ref. 28.

More generally, when there is incomplete expansion of the exhaust flow, the specific impulse I is defined by[29]

$$I = \frac{F}{g_s \frac{dm_p}{dt}} = \frac{v_e}{g_s} + \frac{p_o\left(\frac{p_e}{p_o} - 1\right)A_e}{g_s \frac{dm_p}{dt}}, \tag{33}$$

where v_e is given by Eq. (30). Thus the specific impulse will depend on T_c/M, p_e/p_c, and p_e/p_o. It depends on the height of the rocket through the free-air pressure p_o.

Owing to the presence of the term p_e/p_o, where p_o is a function of altitude, the main question which arises in a rocket motor design, particularly when the motor is to operate over a large variation in p_o, is the determination of the best value to use for p_e. Consider a staged rocket such as the satellite rocket which consists of three burning stages[7]. Since the trajectory of the first stage extends to a height of about 20 miles, the corresponding variation of p_o is very great. However in the second and third stage burning periods the free-air pressure p_o is already so small that its variation is of no significance as far as the operation of the motor is concerned, and for these two stages it is best to design the motor on the basis of $p_o = 0$. The main problem then is that of determining the best design of the rocket motor nozzle for the conditions encountered during the first stage of the burning.

From Eq. (33) it is seen that when the operating conditions are such that v_e is constant and when the burning occurs with constant rate of mass flow of propellants, the specific impulse may be expressed as a linear function of the free-air pressure,

$$I = a - bp_o. \tag{34}$$

The time average of I during the first burning stage is the same as the value of I at the height of the average value of p_o during the first stage. Since the gain in velocity in the trajectory will be greatest when the time average $\bar{I}$ is greatest, it is evident that the best design (best values for a and b) is that for which $\bar{I}$ is greatest. The maximum value of $\bar{I}$ is obtained when the nozzle is designed to give complete expansion, $p_e = \bar{p}_o$ ($\bar{p}_o$ being the time average value of p_o during the first stage), with parallel, one-dimensional, exhaust flow. Thus, the nozzle of the first stage rocket motor should be designed to give complete expansion with parallel exhaust flow for an external pressure having the value $\bar{p}_o$, since, with a fixed exhaust area, this will result in the greatest average thrust over the first stage part of the trajectory. This average value of p_o in the first stage flight is actually about $1/2\ p_{oo}$ (where p_{oo} is the standard sea level pressure). The nozzle thus should be designed to an exit pressure of $1/2\ p_{oo}$ so that at sea level the nozzle is over-expanded. This will cause no difficulty, since even for the most poorly designed nozzles (conical) an over-expansion to $1/4\ p_{oo}$ does not cause shock separation when the expansion angle is as small as the design to be described here. The minimum length of the diverging portion of the exhaust nozzle (3 to 4, Fig. 15) which will give parallel exhaust flow may be determined on the basis of a recent investigation by Guderley[30]. This length is a function of the pressure ratio p_o/p_c, and for the range of pressures of interest here (p_o from 15 to 0 psi, p_c from 150 to 600 psi) it is found that the minimum length to give parallel flow is greater than is desirable for use in the satellite rocket. Letting ℓ_2 denote the length of the diverging section 3 to 4, Fig. 15, and d_t the throat diameter, it is found from combined considerations of weight, thrust, and skin friction that satisfactory values for ℓ_2 are given by $\ell_2 = 2.76\ d_t$ for the first stage and $\ell_2 = 4.25\ d_t$ for the second and third stages[31]. The results of ref. 30 may also be used to determine the loss of thrust which results when the length ℓ_2 is less than that required to give parallel flow; and for the first stage, for example, where $\ell_2 = 2.76\ d_t$, it is found that the loss in thrust is only about 1/2 per cent, which may be absorbed into the general rocket motor efficiency factor.

The methods and results presented in ref. 30 are of considerable importance in rocket motor design. In this paper Guderley shows how the diverging portion of the exhaust nozzle should be designed to give the greatest thrust for various given values of ℓ_2/d_t and for different values of p_o. The analysis, which assumes frictionless flow, is based on a method of three dimensional characteristics combined with the use of the calculus of variations. The rocket motor nozzle shapes and efficiencies for the satellite rocket as determined on the basis of the results of ref. 30 are discussed in ref. 31.

Letting η denote an efficiency factor which includes burning efficiency and friction losses, and using $\dot{w}_p \equiv g_s\ dm_p/dt$ to denote the rate of weight flow of propellants, relation (33) becomes (for parallel flow)

$$\frac{F}{\eta} = \frac{I\ \dot{w}_p}{\eta} = \dot{w}_p v_e + (p_e - p_o)A_e. \tag{35}$$

A thrust coefficient C_F is now introduced as defined by the relation

$$C_F = \frac{F}{\eta\, p_c A_t} = \frac{I\, \dot{w}_p}{\eta\, p_c A_t} = \frac{\dot{w}_p}{p_c A_t}\, v_e + \left(\frac{p_e}{p_c} - \frac{p_o}{p_c}\right) \frac{A_e}{A_t}\,, \tag{36}$$

where A_t is the sectional area at the throat. Letting C_p denote the specific heat at constant pressure, it may be shown that

$$\frac{\dot{w}_p}{p_c A_t}\, v_e = \frac{\rho_t\, v_t}{p_c} \sqrt{2C_p\, T_c \left[1 - \left(\frac{p_e}{p_c}\right)^{\frac{\gamma - 1}{\gamma}}\right]},$$

where the subscript t refers to conditions at the throat. Since the Mach number M_t at the throat is always equal to one, it follows that this may be written in the form (see ref. 19, p. 60)

$$\frac{\dot{w}_p}{p_c A_t}\, v_e = \sqrt{\frac{2\gamma^2}{\gamma - 1} \left(\frac{2}{\gamma + 1}\right)^{\frac{\gamma + 1}{\gamma - 1}}} \sqrt{1 - \left(\frac{p_e}{p_c}\right)^{\frac{\gamma - 1}{\gamma}}}\,. \tag{37}$$

In the special case that $p_e = p_o$, we have

$$C_F = \sqrt{\frac{2\,\gamma^2}{\gamma - 1} \left(\frac{2}{\gamma + 1}\right)^{\frac{\gamma + 1}{\gamma - 1}}} \sqrt{1 - \left(\frac{p_o}{p_c}\right)^{\frac{\gamma - 1}{\gamma}}}\,. \tag{38}$$

Since it is found that the time average of p_o during the first stage of the burning is about half the sea level pressure, which will be denoted by $1/2\ p_{oo}$, if the exhaust nozzle should be designed to give complete expansion at this pressure, the average specific impulse $\bar{I}_1$ during the first stage would be given by

$$\bar{I}_1 = \frac{\eta_1\, p_c\, A_t}{\dot{w}_p} \left[\sqrt{\frac{2\,\gamma^2}{\gamma - 1} \left(\frac{2}{\gamma + 1}\right)^{\frac{\gamma + 1}{\gamma - 1}}} \sqrt{1 - \left(\frac{\frac{1}{2}\, p_{oo}}{p_c}\right)^{\frac{\gamma - 1}{\gamma}}}\right], \tag{39}$$

where, since $\bar{p}_e = \bar{p}_o = 1/2\ p_{oo}$, the average value of the term $(p_e/p_c - p_o/p_c)$ is zero. However, the instantaneous value I_1 of the specific impulse in the first stage will be a function of the external pressure p_o as given by

$$I_1 = \frac{\eta_1\, p_c\, A_t}{\dot{w}_p} \left[\sqrt{\frac{2\,\gamma^2}{\gamma - 1} \left(\frac{2}{\gamma + 1}\right)^{\frac{\gamma + 1}{\gamma - 1}}} \sqrt{1 - \left(\frac{\frac{1}{2}\, p_{oo}}{p_c}\right)^{\frac{\gamma - 1}{\gamma}}}\right] + \left(\frac{\frac{1}{2}\, p_{oo}}{p_c} - \frac{p_o}{p_c}\right) \frac{A_e}{A_t}, \tag{40}$$

where η_1 includes losses in thrust due to burning inefficiency, friction, and a 1/2 % loss because the length ℓ_2 is shorter than that necessary for complete expansion. The value $\eta_1 = 0.90$ has been adopted as a satisfactory description of the rocket motor performance in the first stage. The area ratio is calculated from the relation (ref. 19, p. 60)

$$\frac{A_e}{A_t} = \frac{\left(\frac{2}{\gamma+1}\right)^{\frac{\gamma+1}{2(\gamma-1)}}}{\left(\frac{p_e}{p_c}\right)^{\frac{1}{\gamma}} \sqrt{\frac{2}{\gamma-1}\left[1-\left(\frac{p_e}{p_c}\right)^{\frac{\gamma-1}{\gamma}}\right]}}, \tag{41}$$

where it is understood that $p_e = 1/2\ p_{oo}$ is to be used in the first stage.

Setting $p_o = p_{oo}$, the basic specific impulse I_o, Eq. (32), may also be expressed in the form

$$I_o = \frac{p_c A_t}{\dot{w}_p} \sqrt{\frac{2\gamma^2}{\gamma-1}\left(\frac{2}{\gamma+1}\right)^{\frac{\gamma+1}{\gamma-1}}} \cdot \sqrt{1-\left(\frac{p_{oo}}{p_c}\right)^{\frac{\gamma-1}{\gamma}}} = \frac{p_c A_t}{\dot{w}_p} C_{F_o}. \tag{42}$$

It is now desired to determine the best (optimum) value of the combustion chamber pressure p_c to use in the operation of the rocket motor. This is determined by weighing the increased flight performance (acceleration) which occurs with large p_c against the extra weight which large p_c and large acceleration demand because of the structural strength required. Using $\eta_1 = 0.90$ and comparing (39) and (42), it is evident that

$$\bar{I}_1 = 0.90\ I_o \left[\frac{\sqrt{1-\left(\frac{1}{2}\frac{p_{oo}}{p_c}\right)^{\frac{\gamma-1}{\gamma}}}}{\sqrt{1-\left(\frac{p_{oo}}{p_c}\right)^{\frac{\gamma-1}{\gamma}}}}\right]. \tag{43}$$

By using this expression, $\bar{I}_1$ may be calculated for various combustion chamber pressures p_c using the values of I_o derived in ref. 28 for the different propellant systems. This relation is plotted in Fig. 16 for the hydrazine-oxygen propellant system. The values given here for $\bar{I}_1$, together with those for I_2 and I_3 discussed later, are used to determine the optimum p_c according to the analysis given in the Structure and Weight Report[12].

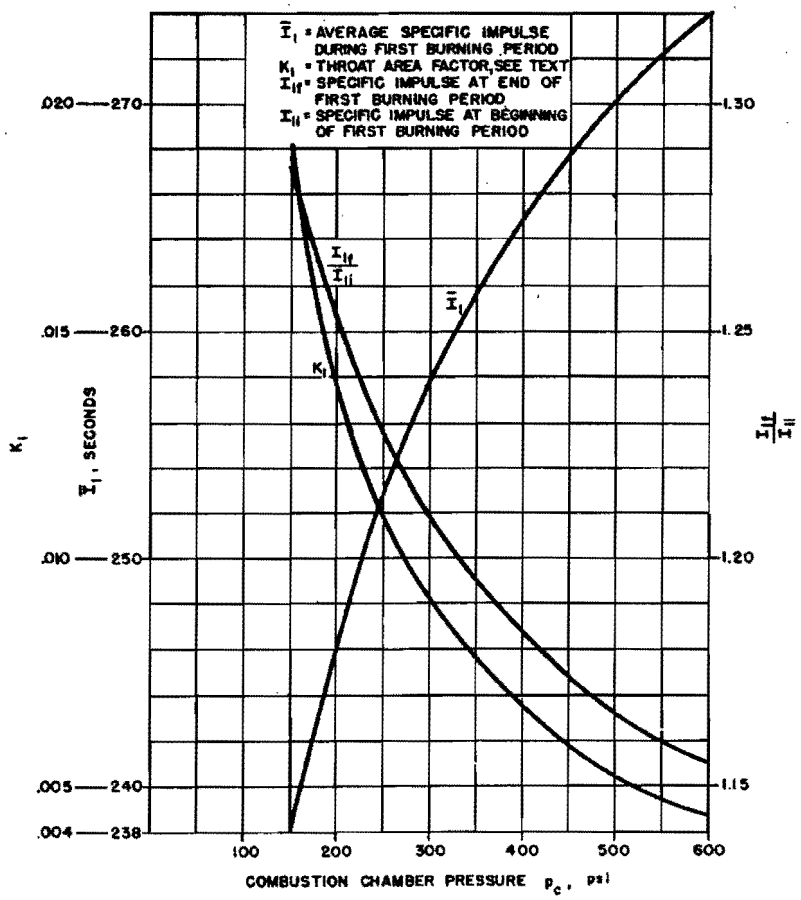

VARIATION OF SEVERAL ROCKET MOTOR PARAMETERS WITH COMBUSTION CHAMBER PRESSURE DURING THE FIRST BURNING PERIOD OF A HYDRAZINE–OXYGEN PROPELLANT SYSTEM

FIG. 16

The investigation of the optimum p_c for least gross weight also requires the relation

$$\frac{I_{1f}}{I_{1i}} = \frac{\left[\sqrt{\frac{2\gamma^2}{\gamma-1}\left(\frac{2}{\gamma+1}\right)^{\frac{\gamma+1}{\gamma-1}}}\sqrt{1-\left(\frac{1}{2}\frac{p_{oo}}{p_c}\right)^{\frac{\gamma-1}{\gamma}}} + \frac{1}{2}\frac{p_{oo}}{p_c}\frac{A_e}{A_t}\right]}{\left[\sqrt{\frac{2\gamma^2}{\gamma-1}\left(\frac{2}{\gamma+1}\right)^{\frac{\gamma+1}{\gamma-1}}}\sqrt{1-\left(\frac{1}{2}\frac{p_{oo}}{p_c}\right)^{\frac{\gamma-1}{\gamma}}} - \frac{1}{2}\frac{p_{oo}}{p_c}\frac{A_e}{A_t}\right]}, \quad (44)$$

where I_{1i} is the specific impulse at the beginning of the first burning period and I_{1f} that at the end of the period. As with Eq. (43), this ratio may also be investigated for various propellants and various p_c. These plots are also shown in Fig. 16.

In order to proceed further with the structural requirements it is necessary to know how A_t varies with p_c and with the propellants used. At the end of the first burning period the thrust is $W_1(1 - \nu)n$ (ref. 7) where W_1 is the gross weight of the first stage, n is the maximum load factor, and ν is the ratio of propellant weight to gross weight. From Eqs. (36) and (40), using $p_o = 0$ at the end of the first burning period, the thrust is also given by

$$F_{1f} = \eta_1 p_c A_t \left[\sqrt{\frac{2\gamma^2}{\gamma - 1}\left(\frac{2}{\gamma - 1}\right)^{\frac{\gamma + 1}{\gamma - 1}}} \sqrt{1 - \left(\frac{1}{2}\frac{p_{oo}}{p_c}\right)^{\frac{\gamma - 1}{\gamma}}} + \frac{1}{2}\frac{p_{oo}}{p_c}\frac{A_e}{A_t} \right], \quad (45)$$

and it therefore follows that

$$A_{t1} = \frac{W_1 (1 - \nu)n}{\eta_1} K_1, \text{ where} \quad (46)$$

$$\frac{1}{K_1} = p_c \left[\sqrt{\frac{2\gamma^2}{\gamma - 1}\left(\frac{2}{\gamma - 1}\right)^{\frac{\gamma + 1}{\gamma - 1}}} \sqrt{1 - \left(\frac{1}{2}\frac{p_{oo}}{p_c}\right)^{\frac{\gamma - 1}{\gamma}}} + \frac{1}{2}\frac{p_{oo}}{p_c}\frac{A_e}{A_t} \right]. \quad (47)$$

The plot of K_1 is included in Fig. 16. The variation of these parameters for the hydrazine-fluorine propellant system is shown in Fig. 17.

In the second and third stages the external pressure p_o is zero as far as the nozzle design is concerned. When the exhaust pressure p_e in the nozzle is zero, it is found that parallel flow can never be obtained no matter how great the distance ℓ_2 is made. In view of this fact, for stages 2 and 3 a reasonable length is chosen for ℓ_2 and the shape is based on results given in ref. 30. The length chosen was approximately 4.2 times the diameter d_t, which gives $A_e/A_t = 15$ approximately. Since the parallel (one dimensional) flow case is so readily calculable and since, for $A_e/A_t = 15$, the difference in efficiency between that for parallel flow and that for the chosen design is only 1.5 per cent, parallel flow is assumed. The 1.5 per cent error thus introduced is absorbed into the efficiency factor $\eta_2 = \eta_3$ which then becomes $\eta_2 = \eta_3 = 0.99\eta_1 = 0.89$, since a 1/2 % loss of this type was already included in the value $\eta_1 = 0.90$. It is now necessary to determine the quantities I_2, I_3, K_2, and K_3 for the second and third stages. On the basis of one-dimensional flow

$$C_{F2} = \sqrt{\frac{2\gamma^2}{\gamma - 1}\left(\frac{2}{\gamma - 1}\right)^{\frac{\gamma + 1}{\gamma - 1}}} \sqrt{1 - \left(\frac{p_e}{p_o}\right)^{\frac{\gamma - 1}{\gamma}}} + \frac{p_e}{p_c}\frac{A_e}{A_t}, \quad (48)$$

where $A_e/A_t = 15$. Now $K_2 = 1/p_c C_{F2}$ and therefore

$$A_{t2} = \frac{W_2 (1 - \nu)n}{\eta_2} K_2. \tag{49}$$

In a similar manner it is shown for the third stage that

$$A_{t3} = \frac{W_3 (1 - \nu)n}{\eta_2} K_3, \tag{50}$$

where $K_3 = K_2$ and $\eta_3 = \eta_2$. Since $I_2 = I_3 = \left(\eta_2 p_c A_{t2}/\dot{w}_{p2}\right) C_{F2}$, and $I_o = \left(p_c A_{to}/\dot{w}_{p2}\right) C_{Fo}$, it follows that

$$I_2 = \eta_2 I_o \frac{C_{F2}}{C_{Fo}} . \tag{51}$$

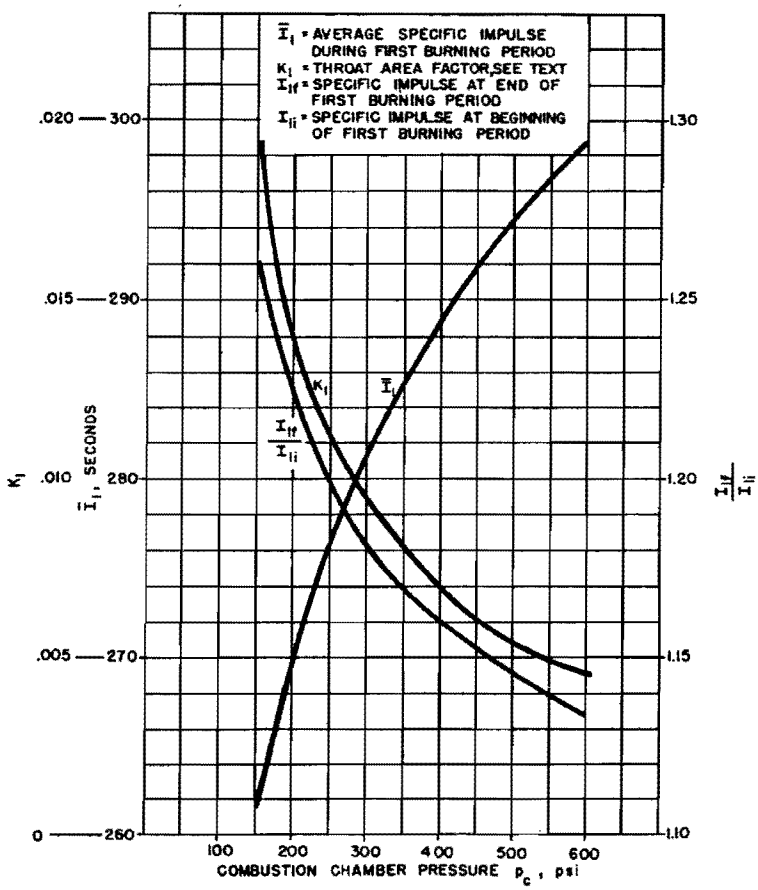

VARIATION OF SEVERAL ROCKET MOTOR PARAMETERS WITH COMBUSTION CHAMBER PRESSURE DURING THE FIRST BURNING PERIOD OF A HYDRAZINE–FLUORINE PROPELLANT SYSTEM

FIG. 17

Using values of I_o and γ from ref. 28, plots of $\bar{I}_1$, I_{1f}/I_{1i}, and K_1, versus p_c as the independent variable are shown in Figs. 16 and 17. Plots of K_2 and I_2 versus p_c are shown in Figs. 18 and 19. These results are used in the Structure and Weight Report[12] along with structural consideration in order to obtain the optimum chamber pressure for which the rocket motor should be designed. The initial structural studies indicated that the optimum values were $p_{c2} = p_{c3} = 150$ psi and $p_{c1} = 400$ psi for the hydrazine-oxygen propellant system. This gives $I_2 = I_3 = 296.7$ and, from Eq. (39) and (42), I_1 becomes

$$I_1 = 0.9\, I_o \left[\frac{\sqrt{1 - \left(\frac{1}{2}\frac{p_{oo}}{p_c}\right)^{\frac{\gamma-1}{\gamma}}}}{\sqrt{1 - \left(\frac{p_{oo}}{p_c}\right)^{\frac{\gamma-1}{\gamma}}}} + \frac{\left(\frac{1}{2}\frac{p_{oo}}{p_c} - \frac{p_o}{p_c}\right)\frac{A_e}{A_t}}{\sqrt{\frac{2\gamma^2}{\gamma-1}\left(\frac{2}{\gamma+1}\right)^{\frac{\gamma+1}{\gamma-1}}\left(1 - \frac{p_{oo}}{p_c}\right)^{\frac{\gamma-1}{\gamma}}}} \right] \quad (51a)$$

Using the optimum value $p_{c1} = 400$ psi and atmospheric density values from ref. 8, the variation of I_1 with height as computed from Eq. (51a) is shown in Fig. 20. These values of I_1 were used in the final trajectory calculations of the Flight Mechanics Report[7]. Also, on the basis of these optimum values found for the p_c, exact shapes were determined[31] for the diverging portion of the exhaust nozzle on the basis of the methods explained in ref. 30. More refined structural studies[12] carried out after these calculations and the trajectory calculations had been completed showed that the optimum p_{c1} was somewhat higher than 400 psi. The optimum value of p_{c2} and p_{c3} remained unchanged. However, since this more accurate value of p_{c1} produces a change in the minimum gross weight of less than 1000 pounds, the use of the value $p_c = p_{c1} = 400$ psi is sufficiently accurate for the analysis.

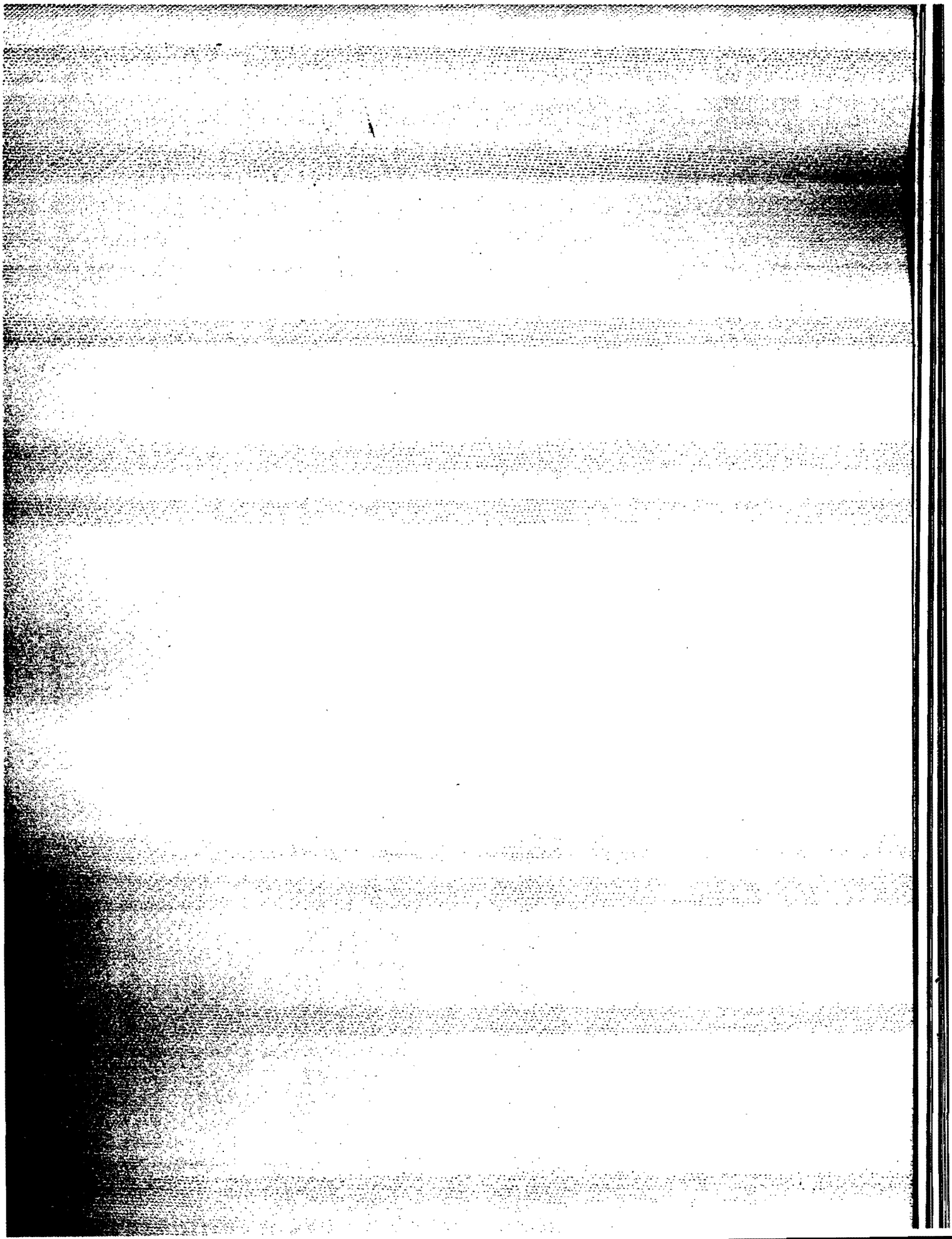

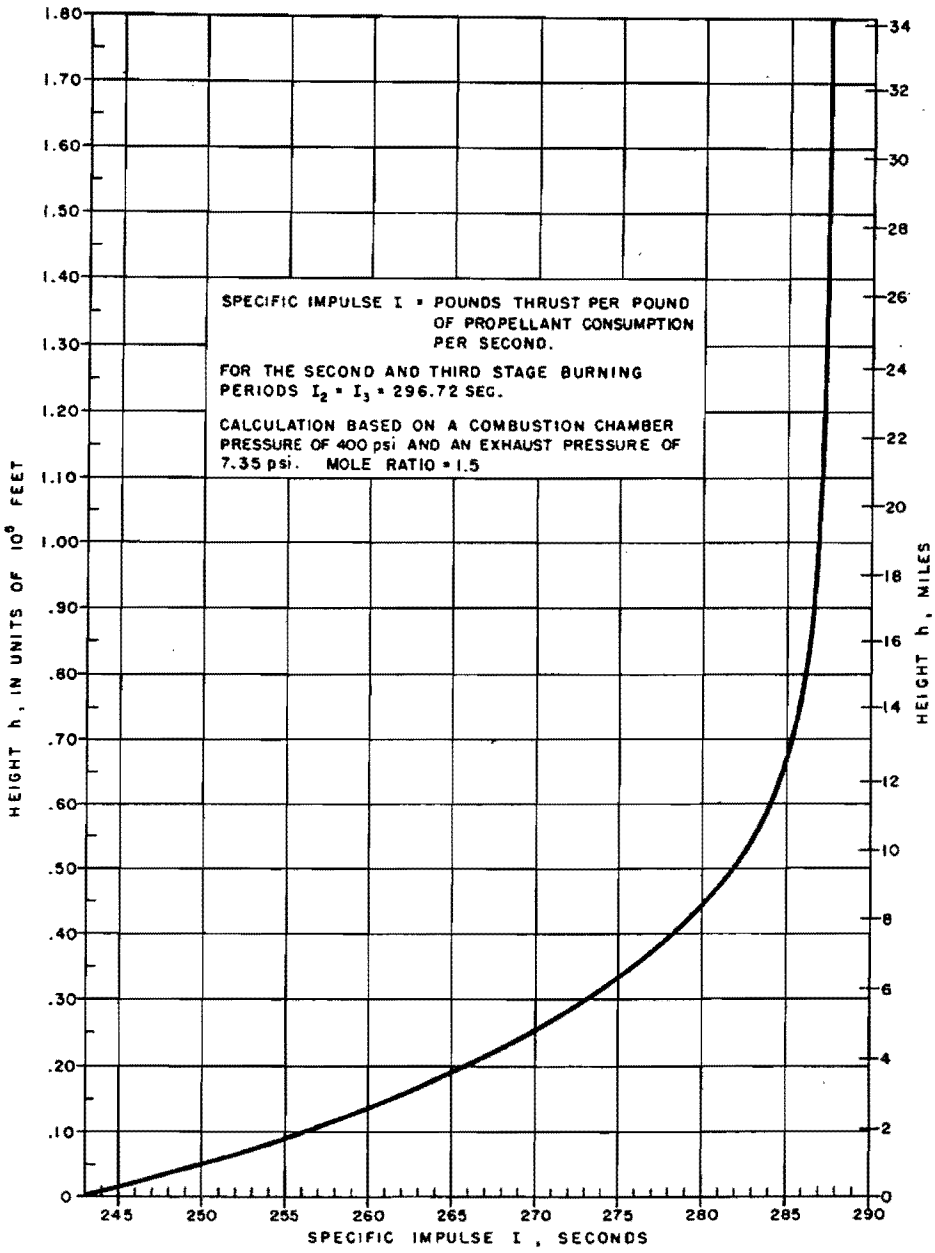

VARIATION OF SPECIFIC IMPULSE WITH HEIGHT DURING THE FIRST STAGE BURNING PERIOD FOR THE HYDRAZINE — OXYGEN PROPELLANT SYSTEM

FIG. 20

B. LIFT FORCES ON A FLAT PLATE AT HIGH MACH NUMBERS FOR USE IN WINGED ROCKET CALCULATIONS

In the early stages of the satellite rocket investigation it appeared that jet vanes might be used for control purposes and accordingly a brief study was made of the lift coefficient of a flat plate at high Mach numbers in order to determine the relation

$$C_L = f(M, \alpha),$$

where C_L is the lift coefficient, M is Mach number, and α is angle of attack. Since jet vanes are situated in the high temperature exhaust flow the calculations were based on $\gamma = 1.25$. However, since results based on this value of γ will not differ greatly from those which would be obtained by using the usual value $\gamma = 1.4$, the jet vane results may be applied to the lifting surfaces of a winged body descending through the atmosphere. For densities which are high enough that the gas dynamical laws are valid and if friction is neglected, the calculations give exact results for any angle of attack and any Mach number provided the shock always remains attached to the leading edge as shown in Fig. 21.

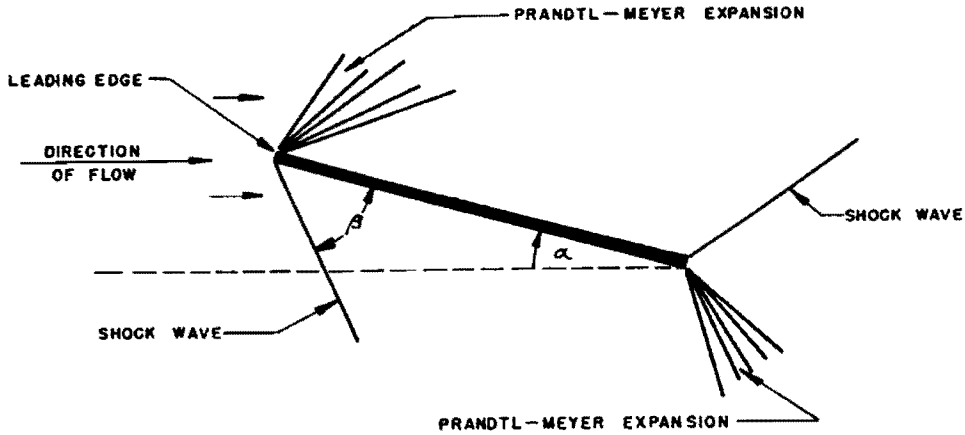

SCHEMATIC DIAGRAM OF FLAT PLATE INCLINED AT AN ANGLE TO SUPERSONIC FLOW

FIG. 21

A single shock wave extends away from the lower surface leading edge while a Prandtl-Meyer expansion occurs at the upper surface leading edge. The pressure on

the upper surface is constant and may be computed by making use of the characteristic equation of supersonic flow (the epicycloid equation). The epicycloid solution for supersonic flow is[20, 25]

$$\alpha = B \tan^{-1}\left[\frac{1}{B}\sqrt{\frac{\left(\frac{W}{a^*}\right)^2 - 1}{1 - \left(\frac{\frac{W}{a^*}}{B}\right)^2}}\right] - \tan^{-1}\sqrt{\frac{\left(\frac{W}{a^*}\right)^2 - 1}{1 - \left(\frac{\frac{W}{a^*}}{B}\right)^2}} - B \tan^{-1}\left[\frac{1}{B}\sqrt{\frac{\left(\frac{u_1}{a^*}\right)^2 - 1}{1 - \left(\frac{\frac{u_1}{a^*}}{B}\right)^2}}\right] + \tan^{-1}\sqrt{\frac{\left(\frac{u_1}{a^*}\right)^2 - 1}{1 - \left(\frac{\frac{u_1}{a^*}}{B}\right)^2}}, \tag{52}$$

where α = angle of attack

$B = \sqrt{\frac{\gamma + 1}{\gamma - 1}}$

W = velocity along the upper surface

u_1 = free-stream velocity

$a^* = \sqrt{\frac{2}{\gamma + 1}}\, a_o$

a_o = velocity of sound in the gas at rest.

If p_1 is the free-stream pressure and p_{2u} is the pressure on the upper surface, the ratio of these pressures is

$$\frac{p_{2u}}{p_1} = \left[\frac{1 - \left(\frac{\frac{W}{a^*}}{B}\right)^2}{1 - \left(\frac{\frac{u_1}{a^*}}{B}\right)^2}\right]^{\frac{\gamma}{\gamma - 1}}. \tag{53}$$

The pressure ratio is determined from this relation by first calculating W/a^* from Eq. (52).

The flow on the lower surface goes through a single shock wave and also produces a constant pressure along this surface. The pressure on the lower surface is calculated from the well-known relations for a diagonal shock wave[5]. If $p_{2\ell}$ is the pressure on the lower surface, the pressure and angle relations are

$$\frac{p_{2\ell}}{p_1} = \left[\frac{2\gamma}{\gamma+1} M_1^2 \sin^2\beta - \left(\frac{\gamma-1}{\gamma+1}\right)\right], \tag{54}$$

$$\tan\alpha = \frac{\frac{v_2}{a^*}}{\frac{u_2}{a^*}}, \tag{55}$$

$$\sin\beta = \frac{\frac{u_1}{a^*} - \frac{u_2}{a^*}}{\left[\left(\frac{u_1}{a^*} - \frac{u_2}{a^*}\right)^2 + \left(\frac{u_2}{a^*}\right)^2\right]^{\frac{1}{2}}}, \tag{56}$$

and

$$\frac{u_1}{a^*} = \frac{M_1\sqrt{\frac{\gamma+1}{2}}}{\sqrt{1+\frac{\gamma-1}{2}M_1^2}}. \tag{57}$$

M_1 is the free-stream Mach numbers, β is the shock angle, u_2 is the horizontal component of the velocity along the lower surface, and v_2 is the vertical component. The vertical component v_2/a^* is connected with the horizontal component u_2/a^* by the strophoid relation

$$\left(\frac{v_2}{a^*}\right)^2 = \frac{\left(\frac{u_1}{a^*} - \frac{u_2}{a^*}\right)^2 \left(\frac{u_1}{a^*}\frac{u_2}{a^*} - 1\right)}{1 - \frac{u_1}{a^*}\frac{u_2}{a^*} + \frac{2}{\gamma+1}\left(\frac{u_1}{a^*}\right)^2}. \tag{58}$$

Computing the pressure according to these formulas and evaluating the lift coefficient from the relation

$$C_L = \frac{\left(\frac{p_{2\ell}}{p_1} - \frac{p_{2u}}{p_1}\right)\cos\alpha}{\frac{\gamma}{2}M_1^2}, \tag{59}$$

we obtain the results shown in Fig. 22.

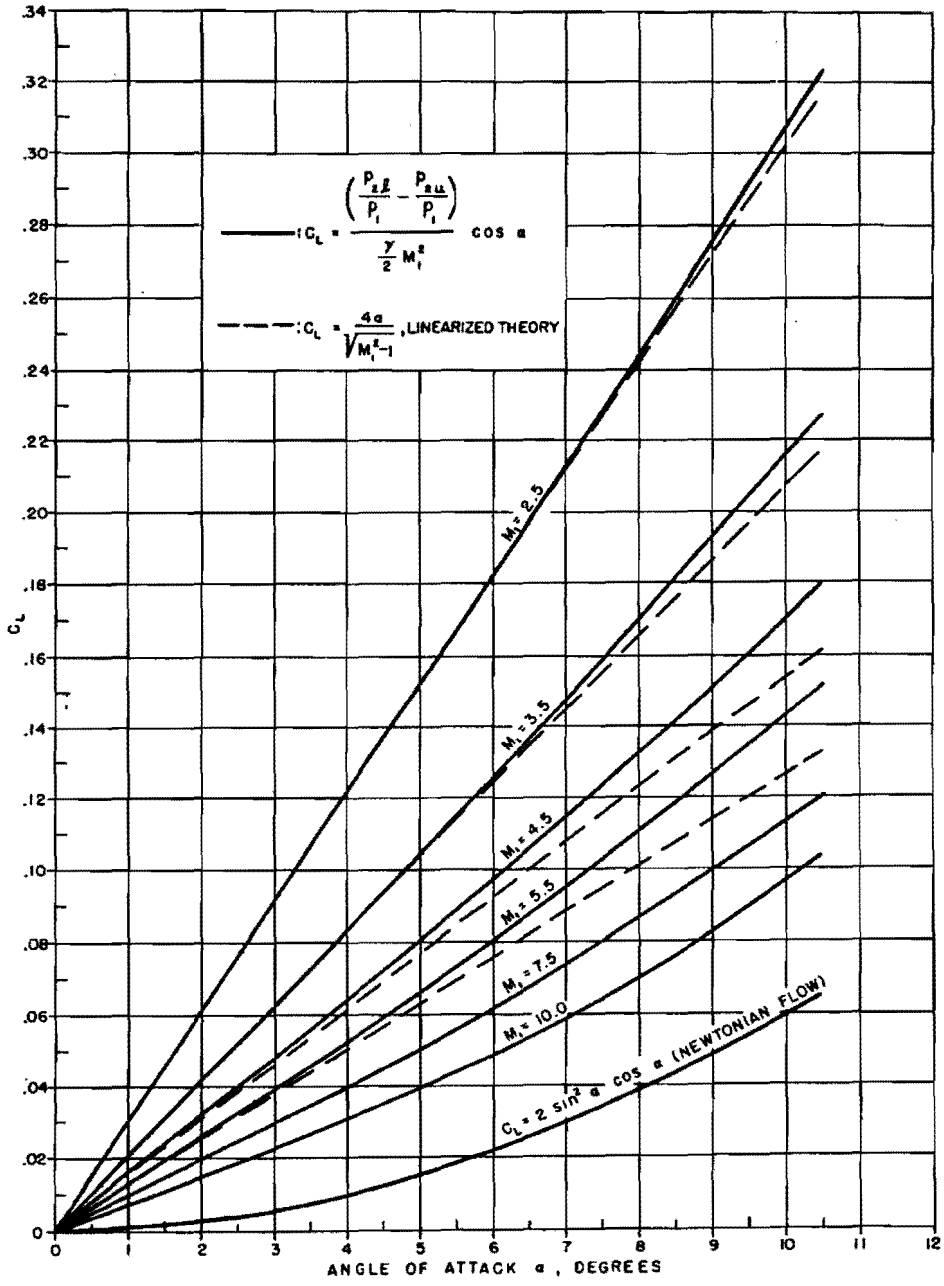

LIFT COEFFICIENT OF A FLAT PLATE AS A FUNCTION OF ANGLE OF ATTACK AND MACH NUMBER

FIG. 22

III. HEAT TRANSFER

Owing to the rather extreme conditions under which a satellite rocket must operate, several important heat transfer problems require serious consideration. These problems may be separated into three categories: (1) those connected with the high speed air flow over the external surface of the rocket (skin temperature), (2) those connected with the high speed flow of the propellants through the propellant system, and (3) the flow of the high temperature products of combustion through the exhaust nozzle (cooling of the rocket motor). In the discussion here, only the heat transfer problems arising in connection with the skin temperature (external flow) will be treated. Thus, a very important heat transfer problem arising in connection with the external flow over the satellite rocket is that of determining the maximum skin temperature produced by atmospheric friction resulting from the very high speed flight of the rocket, not only over its ascending trajectory but also during the descent. Once the satellite has been established on its orbit, a further problem is that of determining the variations in temperature of the skin resulting from radiation processes.

A. SKIN TEMPERATURES DURING ASCENT OF THE SATELLITE ROCKET AND DESCENT OF THE SATELLITE BODY

It is found that the maximum skin temperature during the trajectory ascent occurs at heights where the Reynolds number still predicts laminar flow. Actually this is the so-called region of slip flow, Tsien[10], where the mean free path l of the atmospheric gas particles is no longer negligible compared to the length of the body. In the study here it will be assumed that the slip flow region is bounded by $l/\ell_0 = 0.1$, and that for $l/\ell_0 > 1$ free molecule flow exists. As in the drag investigation, it will be assumed that the gas dynamical laws are valid during the ascent, at least up to those heights where the Reynolds number still predicts laminar flow, i.e., $Re \geq 100$.

The important physical processes determining the skin temperature are the forced convection of heat from the boundary layer to the skin and the loss of heat from the skin resulting from its emitted radiation. There would also be some heat conducted through the skin to the inside of the rocket, but since this would be difficult to specify, it will be neglected. This neglect gives a conservative (high) value for the skin temperature. On the basis of the first law of thermodynamics the equation for the heat transfer per unit time and per unit surface area is

$$C\frac{m}{S}\frac{dT_w}{dt} = h(T_i - T_w) - \sigma\epsilon\left[\left(\frac{T_w}{100}\right)^4 - \left(\frac{T_{oo}}{100}\right)^4\right] , \qquad (60)$$

where C = specific heat of the metal skin which is composed of stabilized 18-8 type stainless steel. The thickness of the skin is 0.020 inch.

$\frac{m}{S}$ = mass of metal skin per unit surface area

T_w = the instantaneous absolute skin temperature (i.e. wall temperature)

T_i = inherent temperature of the skin when it is in thermal equilibrium with the boundary layer

t_{oo} = standard sea-level temperature of the atmosphere

t = time

h = average heat transfer coefficient over a length of wall ℓ_w, per unit area per unit time

σ = Stefan-Boltzmann radiation constant = 0.174 $\dfrac{\text{Btu}}{\text{hour ft}^2 \left(\dfrac{^\circ R}{100}\right)^4}$

ϵ = emissivity of metal skin.

The first term on the right represents the forced convection and the second term the radiation. The variation of the specific heat C with temperature is shown in Fig. 23.

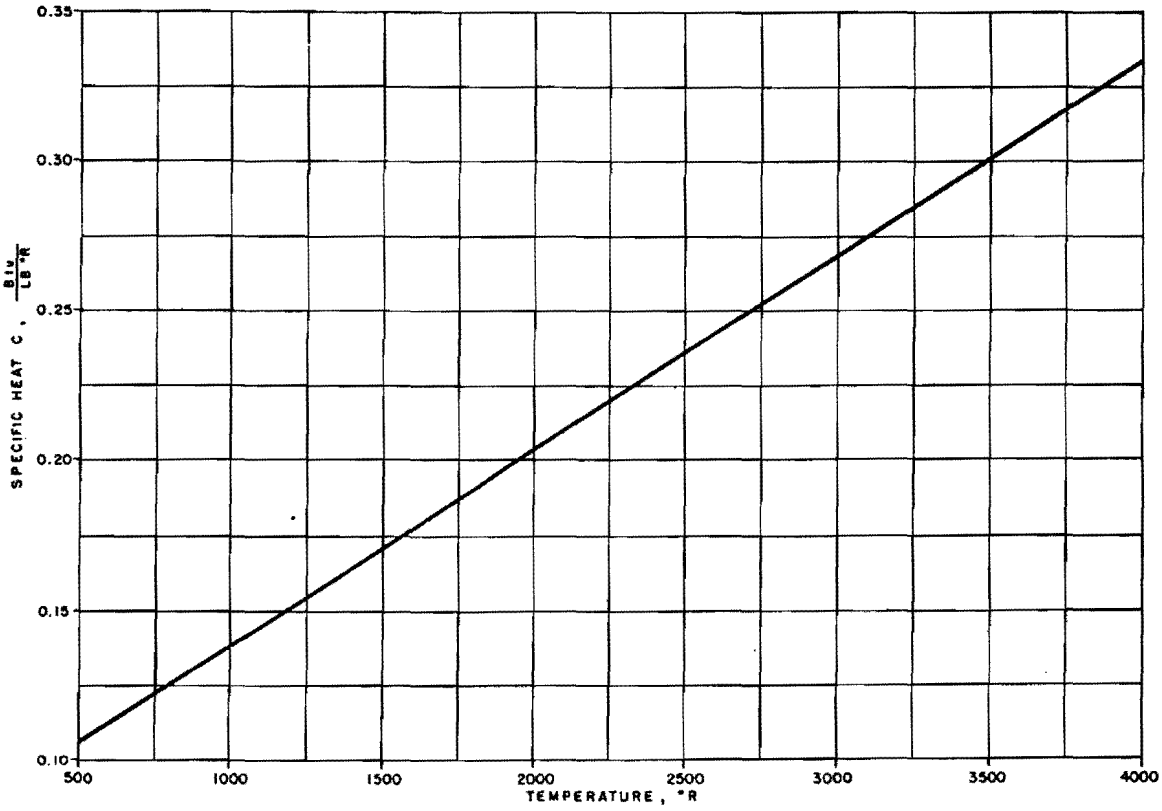

VARIATION WITH TEMPERATURE OF THE SPECIFIC HEAT OF STABILIZED 18-8 TYPE STAINLESS STEEL

FIG. 23

The term $\sigma\epsilon (T_{oo}/100)^4$ is supposed to represent adequately the radiation received by the skin from the sun, the atmosphere, and the earth when the rocket is travelling over a trajectory. Strictly speaking, at low altitudes T_{oo} should be replaced by the free-air temperature T_o at the given altitude. At high altitudes the temperature used should be that which would result from solar insolation alone. However, since this does not differ greatly from the sea level atmospheric temperature (see Fig. 25 for example), the value T_{oo} will be used. On the other hand the use of T_o for the skin temperature at heights of the order of 70-80 miles would be quite erroneous since, although the atmospheric gas has a high kinetic temperature at these heights, the atmosphere is so rarefied that the effect of its temperature in determining the temperature of the skin is entirely negligible. The error introduced in the maximum skin temperature determination by using T_{oo} instead of T_o is very small, about 20°F.

In the forced convection term T_i is the inherent temperature of the skin which in general differs from the total or stagnation temperature just outside the boundary layer. For example when the Prandtl number, $P_r = C_p\mu/k$, is different from 1.0, the inherent temperature is less than the total temperature. C_p is the specific heat of air at constant pressure, μ is the absolute viscosity, and k is the thermal conductivity of air. For discussing heat transfer calculations and test results, Eckert[32] finds it convenient to use the formula

$$1 - \Gamma = \frac{T_T - T_i}{T_T - T_g} , \tag{61}$$

where Γ is defined by the ratio

$$\Gamma = \frac{T_i - T_g}{T_T - T_g} . \tag{61a}$$

In these expressions $T_T = T_o [1 + (\gamma-1)M^2/2]$ is the total temperature, T_o is the free-air temperature, M is the flight Mach number, and T_g is the local moving gas temperature in the flow just outside the boundary layer. Eckert[32] gives $\Gamma = 0.96$ for a turbulent boundary layer and $\Gamma = 0.85$ for one which is laminar. Considering the degree of accuracy of the calculations, it is quite permissible to use the value $\Gamma = 1.0$ since this will result in an error in the maximum skin temperature of only about 50°F, which is quite negligible.

On the basis of German experimental data Eckert[32] finds, for turbulent flow, the empirical relation

$$Nu = \frac{h\ell_x}{k} = 0.03(Re)^{0.8} , \tag{62}$$

and that this relation is valid for subsonic as well as supersonic flow. In this expression Nu is the Nusselt number, h is average value of the heat transfer coefficient over the length ℓ_x from the leading edge (in this case the forward end of the nose), and Re is the Reynolds number. The pressure and velocity used in evaluating Re are the local values just outside the boundary layer. The above result, Eq. (62), is in agreement with work done in this country by Martinelli, Tribus, and Boelter[33]. Eber[34], on the other hand, finds a value for Nu in the supersonic region

which is about half that given by Eckert's formula (62), but since this work was done in the transition region from laminar to turbulent flow, these results are discarded in favor of Eckert's results. It is important to point out that the formulas of Eckert and Martinelli give temperatures about twice that which would be given if the formula of Eber were used. The temperatures derived here will therefore lean toward relatively high values.

Using formula (62) by replacing Re in terms of its definition, $Re = \rho_w v \rho(T,p)/\mu$, and using the values $k = 6.87 \times 10^{-5}(T)^{0.86}$ Btu/hr ft °R, and $\mu = 1.259 \times 10^{-12}(T)^{0.71}$ lb hr/ft^2, we obtain

$$h = \frac{11.5}{(\rho_w)^{0.2}(T)^{0.513}} \left(u\frac{p}{p_{oo}}\right)^{0.8}, \tag{63}$$

where u represents the local velocity of flow just outside the boundary layer, and p is the corresponding pressure. The atmospheric pressure at sea level is denoted by p_{oo}. The manner in which T is to be interpreted is still to be determined. The question is whether T should be interpreted as the boundary layer temperature or the skin temperature when these two differ, as is the case when a transient condition is present. Eckert indicates that the data favor the interpretation of T as the skin (i.e., wall) temperature T_w and since this is also a conservative interpretation, it is the one adopted. The maximum skin temperature when based on this value, $T = T_w$, is 200°R higher than when T_T is used.

For laminar boundary layer flow the heat transfer formula is

$$h = \frac{0.765}{(\rho_w)^{0.5}} \quad u\left(\frac{p}{p_{oo}}\right)^{0.5}. \tag{64}$$

This formula is used for $Re < 2.9 \times 10^5$, where the Reynolds number is computed from

$$Re = 27.3 \times 10^7 \quad \frac{\rho_w}{(T_w)^{1.71}} \left(\frac{p}{p_{oo}} u\right). \tag{65}$$

For $Re > 2.9 \times 10^5$ the formula used for the heat transfer coefficient is

$$h = \frac{11.5}{(\rho_w)^{0.2}\ (T_w)^{0.513}} \left(\frac{p}{p_{oo}} u\right)^{0.8} - 0.021 \frac{(T_w)^{0.855}}{\rho_w}, \tag{66}$$

where the second term on the right is present in order to take account of the laminar boundary layer on the forward portion of the nose. The pressure p is the local pressure just outside the boundary layer and is evaluated from the Taylor-Maccoll cone theory[4]. At $Re = 2.9 \times 10^5$ the two expressions for h become identical.

The position along the skin of the body where the maximum temperature occurs will be situated, in general, where m/S and ρ_w are small, that is, where h is large. The maximum temperature calculations are therefore carried out for a position near

the forward end of the nose at ℓ_s = 1.2 ft. where m/S = 0.82 lb/ft^2. For this position and using a trajectory very similar to that adopted as optimum in ref. 7, the variation of the skin temperature T_s with time as computed from Eq. 60 is shown in Fig. 24. These values refer only to the lower part of the trajectory (up to about 60 miles) where the gas dynamical laws are assumed to be valid. This is the region in which the high skin temperatures are produced, and it is seen from Fig. 24 that the maximum temperature indicated is of the order of 1300°R. This occurs at a height of about 40 miles. Earlier calculations based on a less steep trajectory had given a maximum temperature of the order of 2000°R.

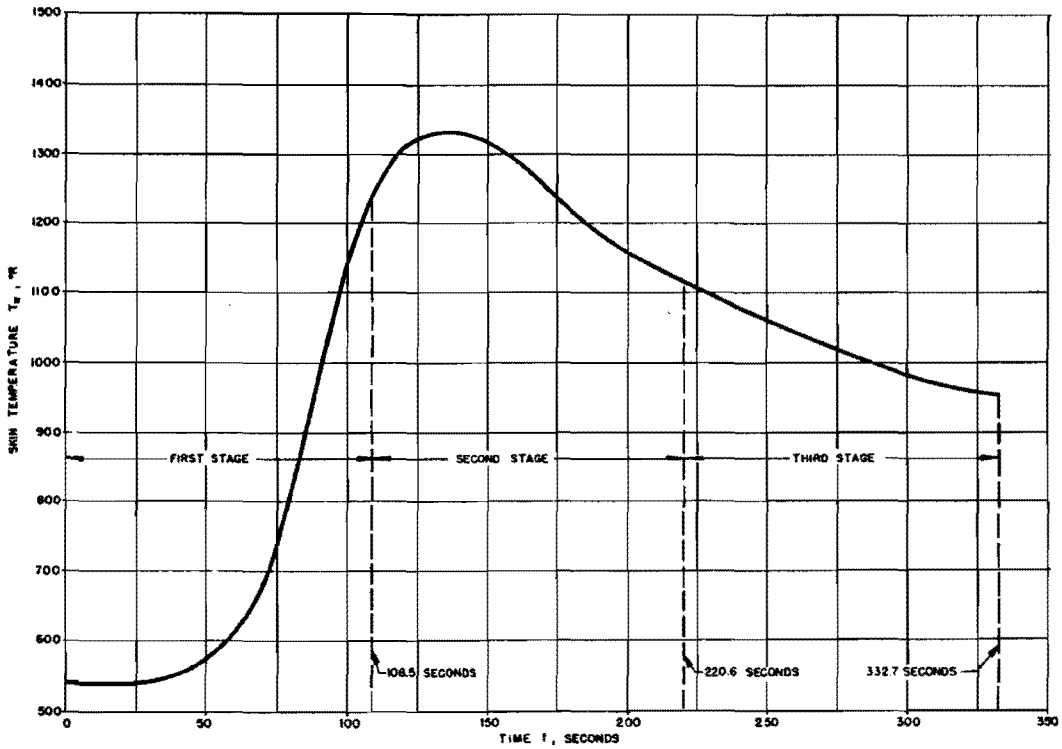

TIME VARIATION OF THE SKIN TEMPERATURE CORRESPONDING TO THE OPTIMUM TRAJECTORY OF THE THREE STAGE HYDRAZINE–OXYGEN SATELLITE ROCKET

FIG. 24

In the rarefied regions of the atmosphere above 80 or 90 miles the heat transfer can no longer be calculated on the basis of the formulas given below but rather must be based on the properties of the free molecule flow mentioned previously in Part I. It was pointed out there that the gas particles are assumed to lose all of their directed kinetic energy upon striking the metal skin of the rocket. The temperature effects resulting from the impacts of the gas particles on the skin may therefore be computed on this basis. At these altitudes (80-90 miles) the third stage of the rocket is operative, and since this has the shape of a cone, the rate mass flow entering the skin (the gas particles are assumed to enter the skin and then be reemitted

diffusely as explained in Part I) is $\rho_o v S \sin\phi$, where ρ_o is the atmospheric density, v is the speed of the rocket, S is the conical surface area, and ϕ is the half angle of the cone.

It is more convenient here to consider the rocket as stationary in a stream of atmospheric gas of velocity v. The velocity v is so large compared to the thermal velocity of the particles that the latter may be neglected, and all particles may then be considered as moving in the same direction, that of the direction of motion v. Since the kinetic energy E per unit mass of atmospheric gas is $1/2\ v^2$, the rate dE/dt at which energy enters the skin of the rocket is

$$\frac{dE}{dt} = \frac{1}{2}\rho_o v^3 \sin\phi \tag{67}$$

On the basis of this equation it is found that at altitudes above 150 miles the temperature effect resulting from the impacts of the gas particles is completely negligible, and the temperature of the skin is determined entirely by radiative heat transfer. It thus follows that only the radiation processes need be considered in calculating the temperature of the skin of the satellite body during its orbital motion at heights of the order of 350 miles.

Before discussing the temperature of the satellite during its orbital motion, brief mention may be made of the temperatures which would result during a descent of the satellite from its orbit. This type of motion was investigated in ref. 7 (Part II, section 11), where it was found that the descent from 350 to 100 miles altitude was quite slow and was attended by very little change in the velocity or in the angle of inclination of the path. Beginning at 100 miles altitude, however, the descent progresses at a more rapid pace, and the rate of descent in the lower portions of the atmosphere where the density becomes appreciable is extremely rapid. This combination of high speed and high density during the lower part of the descent is found to produce very high skin temperatures. In the descent calculations of ref. 7 it was assumed that the satellite was always headed in the direction of the flight path, and the drag from 350 miles down to 80 miles altitude was calculated on the basis of the free molecule theory, using $C_D = 2$ and using the atmospheric density values given in ref. 8. Below the height of 60 miles the drag was calculated on the basis of the usual gas dynamical laws (Taylor-Maccoll theory for the cone). Between 80 and 60 miles interpolated values of C_D were used.

As in the drag calculations where the divergence from orbital conditions was assumed to be negligible down to 100 miles, it is assumed here, in an analogous fashion, that temperature equilibrium exists down to 100 miles. The temperature in this region is therefore calculated from Eq. (60), using the relation

$$h(T_i - T_w) = \frac{1}{2}\rho_o v^3 \sin\phi \tag{68}$$

and the additional condition $dT_w/dt = 0$. Thus at a height of 100 miles, for example, the steady state heat balance equation is

$$\frac{1}{2}\rho_o v^3 \sin\phi = \sigma\epsilon\left[\left(\frac{T_w}{100}\right)^4 - \left(\frac{T_{oo}}{100}\right)^4\right] . \tag{69}$$

The temperature T_{oo} is used in the radiation term because it represents a reasonable value for the average temperature which would result for the body on the basis of radiation processes alone. Using $\epsilon = 0.95$, and the appropriate values $\rho_o = 9.6 \times 10^{-11}$ slug/ft^3, $v = 24{,}070$ ft/sec, and $T_{oo} = 538.8°R$, it is found that $T_w = 687°R$ at 100 miles altitude.

From 100 down to 80 miles altitude the temperature is calculated on the basis of free molecule flow. In this altitude range the variation of temperature with time is larger, and it is necessary to use the differential equation

$$C \frac{m}{S} \frac{dT_w}{dt} = \frac{1}{2} \rho_o v^3 \sin\phi - \sigma\epsilon \left[\left(\frac{T_w}{100} \right)^4 - \left(\frac{T_{oo}}{100} \right)^4 \right] . \qquad (70)$$

At a height of 80 miles where $v = 24{,}090$ ft/sec this gives $T_w = 1060°R$. Since no lift can be produced by free molecule flow, it follows that even if the descending body were equipped with wings, the velocity and therefore the temperature would remain unchanged.

Beginning at a height of about 60 miles, the heat transfer equations (60), (64), and (66), which are based on gas dynamics, are appropriate to use as a first approximation in the determination of the temperature, the approximation becoming more accurate as the regions of higher density are encountered. It may be worthy of note that the use of the ordinary gas dynamics heat transfer equations implies much smaller relative amounts of heat transferred from the air to the skin since, in the gas dynamics region, the air is turned to flow along the surface of the body, thereby retaining a major portion of its total energy.

Between 80 and 60 miles altitude, the temperatures are determined by fairing the values of h above 80 miles into the values found below 60 miles. Although the calculation of the temperature variations below 80 miles has not yet been completed, it is evident that the skin temperatures calculated according to Eq. (60) will be very high. In this case it is appropriate to add further heat transfer terms to Eq. (60) in order to take account of the loss of heat in the boundary layer due to emitted radiation and also due to gaseous dissociation. Recent calculations by Friedman[35] show that the maximum boundary layer temperature when dissociation is taken into account is of the order of 5000-7000°F. In view of this reduction in the maximum boundary layer temperature resulting from dissociation, it appears that it may be possible to avoid melting during the descent of the satellite, especially if a suitable external insulating layer is used. Thus when dissociation effects are taken into account, it is found that the maximum skin temperature during descent will be of the order of 4000-4500°R. In this case it seems quite possible that a protecting layer of magnesium oxide over the outside surface would be sufficient to prevent melting of the skin.

An investigation is under way to determine whether the maximum skin temperature is reduced when the descending satellite body is equipped with wings. The preliminary results of these calculations indicate that by using wings having the same size relative to the body as in high speed airplane design, the descending trajectory may be sufficiently altered that the skin temperatures which result are only half those which would occur when no wings are employed.

B. TEMPERATURE OF THE SATELLITE BODY DURING ITS ORBITAL MOTION

Once the satellite has been established on its orbit, the skin temperature during the orbital motion will be determined entirely by radiation processes. In order to calculate the radiative heat transfer, the following assumptions are made.

1. The solar radiation Q_s consists of parallel rays containing energy of amount*

$$Q_s = 429 \frac{\text{Btu}}{\text{hr ft}^2} . \tag{71}$$

The satellite is always situated in the equatorial plane of the earth which is at a constant inclination of 23.5° to the earth-sun radius vector.

2. The satellite rotates about the earth in the equatorial plane at a constant height h_o and a constant angular velocity ω_o. One side of the satellite always faces the earth, spends half of the period P of rotation on the night side of the earth, and never receives any direct solar radiation.

3. The earth is assumed to radiate as a black body at the temperature of the upper troposphere (420°R) and to have an albedo[37] of 0.43.

As far as the orbital motion is concerned, it is the maximum and minimum temperatures occurring during a period that are of main interest, partly because of their general effect on the satellite body and partly because of possible use of large differences in temperature to operate a heat engine. Therefore, in order to make the differences as large as possible, it will be assumed that the earth side of the body is painted white to make the temperature of this side as low as possible, while the space side will be assumed to have a surface of polished steel to give a temperature as high as possible. The temperature calculations are made separately for the two opposite sides of the rocket by treating these as flat plate surfaces parallel to the instantaneous horizontal and thermally insulated on the sides which face each other (the inside of the rocket).

1. The Temperature of the Earth Side of the Satellite

The appropriate heat transfer equation for the earth side of the satellite is

$$C \frac{m}{S} \frac{dT}{dt} = \sigma \alpha_1 f_1 T_1^4 - \sigma \epsilon T_w^4 + 0.43\, \alpha_2 f_1 Q_s \cos 23.5° \sin \frac{2\pi}{P} t, \tag{72}$$

where

C = specific heat of skin = 0.12 Btu/lb°R

m/S = density of stainless steel skin per unit surface area = 1.35 lb/ft^2

α_1 = absorption coefficient for radiation received from the earth = 0.95, surface painted white

* Based on 1.94 gram cal/cm^{2}minute as the value for the solar constant, see p. 61 of ref. 36.

α_2 = absorption coefficient for solar radiation received by reflection from the earth = 0.14, surface painted white

ϵ = emissivity = 0.95, surface painted white

T_1 = temperature of outer troposphere = 420°R

f_1 = a geometrical radiation factor = $(R_E/r_{orb})^2$

R_E = radius of the earth at the equator = 3963.34 miles

r_{orb} = distance of the orbit from center of the earth = $R_E + h_o$ = 4313.34 miles

h_o = height of orbit above sea level = 350 miles

P = orbital period = $2\pi/\omega_o$ = 95.844 minutes/revolution

ω_o = angular velocity in the orbit referred to a system of reference not rotating with the earth = 1.0926×10^{-3} radians/sec.

In the calculations the initial condition assumed is that the satellite enters the earth's shadow at the time t = 0.

2. The Temperature of the Space Side of the Satellite

The heat transfer equation for the space side of the satellite is

$$C \frac{m}{S} \frac{dT}{dt} = - \sigma \epsilon T_w^4 + \alpha Q_s \cos 23.5° \sin \frac{2\pi}{P} t. \qquad (73)$$

Assuming the surface to be of polished steel, the values ϵ = 0.07 and α = 0.45 are used.

The time variation of the skin temperatures of the two sides, the earth side painted white and the space side of polished steel, is shown in Fig. 25.

Although preliminary calculations of the temperature of a satellite rocket were made in the initial satellite study[38], the assumptions were more simplified than those used here inasmuch as there was no consideration of the time variation as contained in the right hand side of Eqs. (72) and (73). Moreover, the calculations were based upon heat transfer to the entire mass of the rocket, rather than to the skin alone, and therefore yielded temperatures less extreme than those obtained here.

It is seen from Fig. 25 that the temperature difference between the two sides of the satellite is of the order of 300-400°F, and that a maximum temperature of 960°R will occur on the space side, and a minimum temperature of 400°R will occur on the earth side. There appears to be no special objection to these temperature limits. The figure also includes the temperature which results when both sides are painted with lampblack, in which case the values $\alpha_1 = \alpha_2 = \epsilon = 0.95$ are used. It is seen that this results in a general overall decrease in the temperatures and furthermore that in this case it is the space side of the satellite which has the lower minimum (and also the higher maximum) temperature.

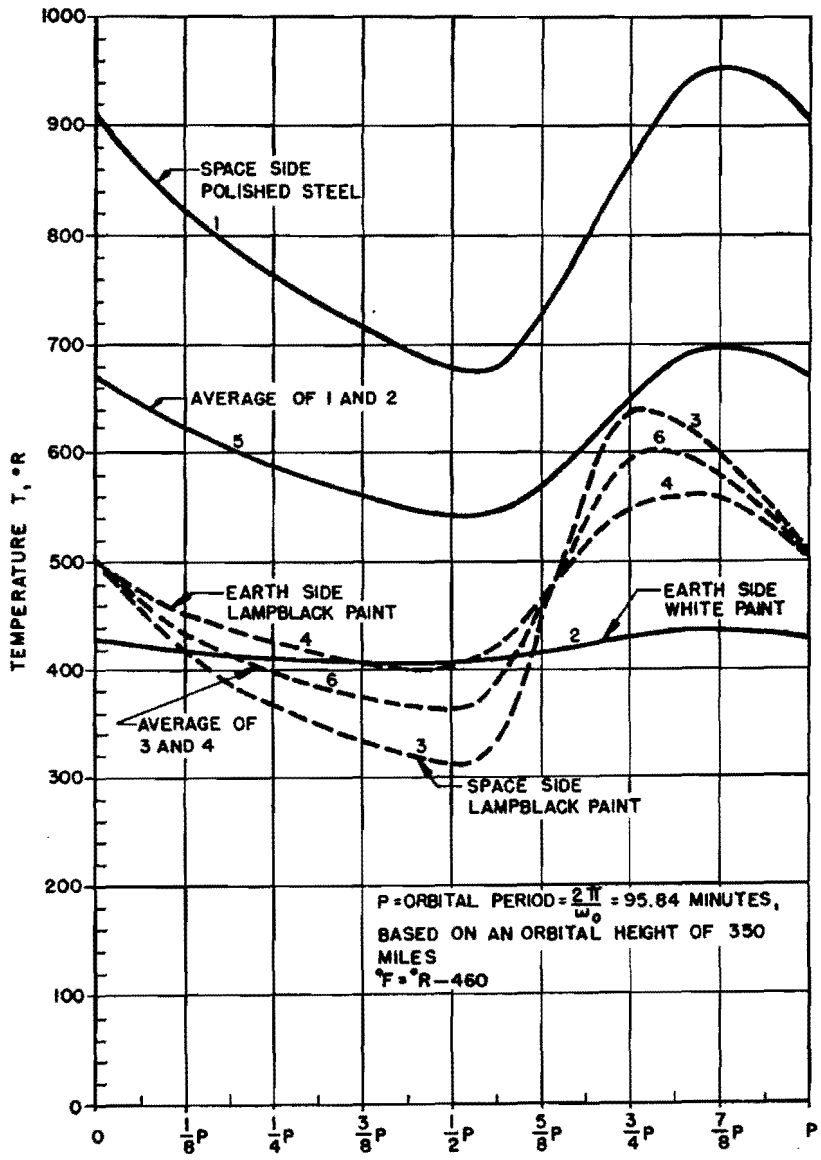

TEMPERATURE OF THE EARTH AND SPACE SIDES OF THE SATELLITE

FIG. 25

APPENDIX

AERODYNAMIC FORCES ON A CONE AT VERY HIGH MACH NUMBERS

At very high Mach numbers the flow is of the Newtonian type[5, 6, 39]; that is, the air strikes the body and loses its normal component of momentum, proceeding along the surface of the body with only its tangential component. Consider a body of revolution with the positive x-axis as the longitudinal axis of symmetry, Fig. 26. The individual surface element at a radial distance r from the longitudinal axis is inclined at an angle ϕ to this axis. The air stream is inclined at an angle α (angle of attack) to the x-axis.

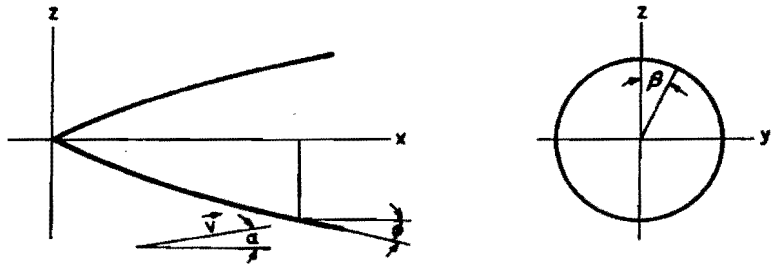

SCHEMATIC DIAGRAM OF BODY OF REVOLUTION INCLINED AT AN ANGLE TO THE FLOW

FIG. 26

The direction cosines of the normal to a surface element $d\sigma$ are $\sin\phi$, $-\sin\beta\cos\phi$, and $-\cos\beta\cos\phi$. The angle η between the velocity vector $\vec{v}$ and the normal to the surface element is given by

$$\cos\eta = \cos\alpha\sin\phi - \sin\alpha\cos\beta\cos\phi \ . \tag{74}$$

The normal component of the velocity is $v_n = v\cos\eta$. The pressure produced at the surface element $d\sigma$ by the momentum loss is given by

$$p = \frac{df}{d\sigma} = \frac{\rho v\, v_n dA}{d\sigma} = \rho v^2\cos^2\eta \ , \tag{75}$$

where df is the force normal to the surface element $d\sigma$, and dA is the projection of the surface element normal to the stream velocity. Using $q = 1/2\ \rho v^2$ we obtain

$$\frac{p}{q} = 2\cos^2\eta. \tag{76}$$

The z-component of the force on the element $d\sigma$ is

$$df_z = - p \cos\beta \cos\phi \, d\sigma = - pr \cos\beta \, d\beta \, dx, \quad (77)$$

while the x-component is given by

$$df_x = p \sin\phi \, d\sigma = pr \tan\phi \, d\beta \, dx \, . \quad (78)$$

The normal and axial forces on the body of revolution per unit length are determined by

$$\frac{dN}{dx} = \int df_z = -2r \int_0^{\pi} p \cos\beta \, d\beta \quad (79)$$

for the normal force, and

$$\frac{dX}{dx} = \int df_x = 2r \tan\phi \int_0^{\pi} p d\beta \quad (80)$$

for the axial force.

Using the non-dimensional representation, we may write

$$C_N' = \frac{dC_N}{d(x/d)} = \frac{1}{\pi q R^2} \frac{dN}{d(x/d)} = -\frac{4}{\pi} \frac{r}{R} \int_0^{\pi} \frac{p}{q} \cos\beta \, d\beta = 2 \frac{r}{R} \sin 2\phi \sin 2\alpha, \quad (81)$$

where $R = d/2$ is the maximum radius of the body.

Similarly, for the axial force we have

$$C_X' = \frac{dC_X}{d(x/d)} = \frac{4}{\pi} \frac{r}{R} \tan\phi \int_0^{\pi} \frac{p}{q} \, d\beta = 4 \frac{r}{R} \tan\phi \, [2\sin^2\phi + \sin^2\alpha \, (1 - 3\sin^2\phi)]. \quad (82)$$

For a conical portion of the body where ϕ = const. and $r = x\tan\phi$, we obtain

$$C_N = \cos^2\phi \sin 2\alpha \, , \quad (83)$$

and

$$C_X = 2 \sin^2\phi + \sin^2\alpha \, (1 - 3 \sin^2\phi) \quad (84)$$

for the normal and axial force coefficients.

REFERENCES

[1] Göthert, B : Private Communication from B. Göthert, Dec., 1946. Also see DVL-JF72913, microfilm reel ADIK-109.

[2] ——— Peenemünde-Kochel Archive, Series 66 reports.

[3] Wall, D.D.: Drag of Three Bodies of Revolution At Supersonic Speeds As A Function of Fineness Ratio. Report SM-20087, Douglas Aircraft Co., Jan., 1946.

[4] Taylor, G.I. and Maccoll, J.W.: The Air Pressure on a Cone Moving At High Speeds. Proc. Roy. Soc., Series A, Vol. 139, 1933, pp. 278-311.

[5] Zahm, A.F.: Superaerodynamics. Journal of the Franklin Institute, Vol. 127, No. 2, Feb., 1934, p. 153.

[6] Epstein, P.: The Resistance of Projectiles At High Mach Numbers. Proceedings of the National Academy of Sciences, Vol. 17, 1931, p. 546.

[7] Krueger, R.W., Grimminger, G., and Tieman, E.M.: Flight Mechanics of a Satellite Rocket. RA-15021, Project RAND, Douglas Aircraft Co., Inc., Feb. 1, 1947.

[8] Grimminger, G.: Analysis of Temperature, Pressure, and Density in the Atmosphere Extending to Extreme Altitudes. RA-15023, Project RAND, Douglas Aircraft Co., Inc., Feb. 1, 1947.

[9] Sänger, E.: Gas Kinetics of Very High Flying Speeds. Deutsche Luftfahrtforschung, Bericht 972, Berlin, 1938. German Translation No. 369, Douglas Aircraft Co., Inc.

[9a] Sänger, E. and Bredt: A Rocket Drive for Long Range Bombers. Deutsche Luftfahrtforschung. Untersuchungen u. Mitteilungen, Nr. 3538, Berlin, 1944. Translation CGD-32, Bureau of Aeronautics, Navy Department, Wash., D.C.

[10] Tsien, H.S.: Superaerodynamics, Mechanics of Rarefied Gases. Journal of Aeronautical Sciences, Vol. 13, No. 12, Dec., 1946.

[11] Cope, W.F.: The Laminar Boundary Layer in Compressible Flow. National Physical Laboratory Report to the Ordnance Board. British Secret Report dated Nov., 1943.

[11a] Cope, W.F.: The Turbulent Boundary Layer in Compressible Flow. National Physical Laboratory Report to the Ordnance Board. British Secret Report dated Nov., 1943.

[12] Clement, G.: Structural and Weight Studies of a Satellite Rocket. RA-15026, Project RAND, Douglas Aircraft Co., Inc., Feb. 1, 1947.

[13] Erdmann: Druckverteilungsmessung am A4VIP im Bereich der Unter-und Überschallgeschwindigkeiten. Peenemünde Archive Nr. 66/100.

[14] Ferri, Antonio: Supersonic-Tunnel Tests of Projectiles in Germany and Italy. NACA Wartime Report L-152, October, 1945.

[15] Tsien, H.S.: Supersonic Flow over an Inclined Body of Revolution. Journal of Aeronautical Sciences, Vol. 5, 1938, pp. 480-483.

[16] Lin, C.C.: Supersonic Lift and Moment Characteristics of a Shell with Conical Nose. Report No. 4-14, Jet Propulsion Laboratory, GALCIT, California Institute of Technology, Pasadena, Calif., Oct., 1945.

[17] Jones, Robert T.: Properties of Low-Aspect-Ratio Pointed Wings at Speeds Below and Above the Speed of Sound. NACA Technical Note 1032, March, 1946.

[18] Frick, R.H.: Stability and Control of a Satellite Rocket. RA-15025, Project RAND, Douglas Aircraft Co., Inc., Feb. 1, 1947.

[19] Jet Propulsion Laboratory and the Guggenheim Aeronautical Laboratory, California Institute of Technology: Jet Propulsion, 1946, Restricted.

[20] Busemann, A.: Gasdynamik. Handbuch der Experimentalphysik, Vol. 4, Akademische Verlagesellschaft, Leipzig, 1931.

[21] Ackeret, J.: Gasdynamik. Handbuch der Physik, Vol. 7, Springer, Berlin, 1931.

[22] Prandtl, L. and Tietjens, O.G.: Fundamentals of Hydro- and Aeromechanics. Chap. XV. McGraw Hill, 1934.

[23] Vogelpohl, G.: Über den Impulssatz der Strömungslehre. Forschung, Band 8, Heft 1, 1937, pp. 35-41.

[24] Malina, F.J.: Characteristics of the Rocket Motor Unit Based on the Theory of Perfect Gases. Journal of the Franklin Institute, Vol. 23, No. 4, 1940, p. 448.

[25] Applied Mathematics Group, New York University: Supersonic Flow and Shock Waves. Applied Mathematics Panel of the NDRC, AMP Report 38.2R, 1944, p. 251-252. Confidential.

[26] Lemmon, A.W. Jr.: Fuel Systems for Jet Propulsion. Appendix 1. Jet Propelled Missiles Panel, Washington, D.C., May, 1945.

[27] Gilliland, E.R.: Rocket-Powered Missiles. Appendix 1. Jet Propelled Missiles Panel, Washington, D.C., May, 1945.

[28] Krieger, F.J.: Theoretical Characteristics of Several Liquid Propellant Systems. RA-15024, Project RAND, Douglas Aircraft Co., Inc., Feb. 1, 1947.

[29] Section H, Division 3, NDRC: Rocket Fundamentals. ABL-SR4, OSRD No. 3992, 1944, p. 23. Confidential.

[30] Guderley, G. and Hantsch, E.: Beste Formen für Achsensymmtrische Uberschallschubdüsen. Unpublished paper furnished by G. Guderley, Dec., 1946.

[31] Gendler, S.L.: Satellite Rocket Power Plant. RA-15027, Project RAND, Douglas Aircraft Co., Inc., Feb. 1, 1947.

[32] Eckert, E.R.G.: Heat Transmission of Bodies in Rapidly Flowing Gases. AAF-IRE Translation No. 46, Feb., 1946, Wright Field, Ohio.

[33] Martinelli, R.C., Tribus, M., and Boelter, L.M.K.: An Investigation of Aircraft Heaters I - Elementary Heat Transfer Considerations in an Airplane. NACA Wartime Report W-23, Oct., 1942.

[34] Eber,: Experimental Investigation of the Drag Temperature and the Heat Transfer on Simple Bodies at Supersonic Speeds - Part I. Archive No. 66/57. German Translation No. 337, Douglas Aircraft Co., Inc.

[35] Friedman, J.: Calculation of Theoretical Stagnation Temperatures of Air. Aerophysics Laboratory Memorandum No. 54, North American Aviation, Inc., Nov., 1946. Restricted.

[36] Brunt, D.: Physical and Dynamical Meteorology. The MacMillan Co., 1934, p. 18.

[37] Humphreys, W.J.: Physics of the Air. McGraw-Hill, 1929, p. 84.

[38] Douglas Aircraft Co., Inc.: Preliminary Design of an Experimental World-Circling Spaceship. Report SM-11827, May, 1946, pp. 170-177.

[39] Karman von, T.: The Problem of Resistance in Compressible Fluids. Volta Conference, Reale Accademia D'Italia, Rome, Vol. XIV, 1936.

INITIAL EXTERNAL DISTRIBUTION LISTS

Initial distribution of all related technical reports on the satellite vehicle is given below. The code is explained on pages 63 through 72.

Report No.	*Title*	*Distribution*
RA-15021	Flight Mechanics of a Satellite Rocket	A(1), C, D(1)
RA-15022	Aerodynamics, Gas Dynamics and Heat Transfer Problems of a Satellite Rocket	A(1), C, D(1)
RA-15023	Analysis of Temperature, Pressure and Density of the Atmosphere Extending to Extreme Altitudes	A(1), C, D(1)
RA-15024	Theoretical Characteristics of Several Liquid Propellant Systems	A(1), C, D(3)
RA-15025	Stability and Control of a Satellite Rocket	A(1), C, D(1), D(2)
RA-15026	Structural and Weight Studies of a Satellite Rocket	A(1), C, D(1)
RA-15027	Satellite Rocket Power Plant	A(1), C, D(3)
RA-15028	Communication and Observation Problems of a Satellite	A(1), C, D(2)
RA-15032	Reference Papers Relating to a Satellite Study	A(1), C, D(2)

Those agencies not on the initial distribution may obtain reports on a loan basis by writing to: Commanding General, Air Materiel Command, Attn: TSEON-2, Wright Field, Dayton, Ohio.

A (1). GOVERNMENT AGENCIES

Guided Missiles Committee
Joint Research & Development Board
New War Department Building
Washington, D.C.

Commanding General (4 Copies)
Army Air Forces
Washington 25, D.C.
Attention: AC/AS-4, DRE-3, Pentagon

Commanding General (25 Copies)
Air Materiel Command
Wright Field, Dayton, Ohio
Attention: TSEON-2

Commanding General
Air University
Maxwell Field, Alabama
Attention: Air University Library

Chief of the Bureau of Aeronautics (6 Copies)
Navy Department
Washington 25, D.C.
Attention: TD-4

Chief of the Bureau of Ordnance (4 Copies)
Navy Department
Washington 25, D.C.
Attention: Re-9

Chief of the Bureau of Ships (3 Copies)
Navy Department
Washington 25, D.C.
Attention: Code 633

Chief, Guided Missiles Branch
Technical Command
Edgewood Arsenal, Maryland

Commanding General
Proving Ground Command
Eglin Field, Florida
Attn: First Experimental Guided Missiles Group

Commanding Officer (2 Copies)
Office of Naval Research Branch Office
616 Mission St.
San Francisco, California

Commanding Officer
U.S. Naval Air Missile Test Center
Point Mugu, California

Commanding Officer
U.S. Naval Ordnance Test Station
Inyokern, California

Commanding Officer
Alamogordo Army Air Base
Alamogordo, New Mexico

Director, National Advisory Committee
for Aeronautics (4 Copies)
1500 New Hampshire Avenue, N.W.
Washington, D.C.
Attention: Mr. C.H. Helms

Director, Naval Research Laboratory (3 Copies)
Anacostia Station
Washington, D.C.

Library of Congress (2 Copies)
Technical Information Section
Washington 25, D.C.
Attention: Mr. J. Heald

Office of the Chief of Ordnance
Ordnance Research & Development Division
Rocket Branch
Pentagon
Washington 25, D.C.

Chief of Naval Operations
Navy Department
Washington 25, D.C.
Attention: Op-57

C. PRIME CONTRACTORS

CONTRACTOR	TRANSMITTED VIA	COGNIZANT AGENCY
Applied Physics Laboratory Johns Hopkins University Silver Spring, Maryland Attn: Dr. Dwight E. Gray (3 copies)	Development Contract Officer Applied Physics Laboratory Johns Hopkins University 8621 Georgia Avenue Silver Spring, Maryland	BUORD
Bell Aircraft Corporation Niagara Falls, New York Attn: Mr. R. H. Stanley Mr. B. Hamlin	Bureau of Aeronautics Rep. Cornell Aeronautical Lab. Box 56 Buffalo, New York	AAF BUAER & BUORD
Bell Telephone Laboratories Murray Hill, New Jersey Attn: Dr. W. A. MacNair		ORD DEPT
Bendix Aviation Corporation Special Products Development, East Teterboro, New Jersey Attn: Dr. Harner Selvidge		AAF & BUORD

C. PRIME CONTRACTORS (Cont'd)

CONTRACTOR	TRANSMITTED VIA	COGNIZANT AGENCY
Boeing Aircraft Company Seattle 14, Washington Attn: Mr. R. H. Nelson		AAF
Consolidated-Vultee Aircraft Corp. Lone Star Laboratory Daingerfield, Texas Attn: Mr. J. E. Arnold	Development Contract Officer Consolidated-Vultee Aircraft Corp. Daingerfield, Texas	BUORD
Consolidated-Vultee Aircraft Corp. Downey, California Attn: Mr. W. M. Robinson	Representative-in-Charge, BUAER Consolidated-Vultee Aircraft Corp. Vultee Field Downey, California	AAF BUAER & BUORD
Cornell Aeronautical Lab. Buffalo, New York Attn: Mr. W. M. Duke	Development Contract Officer Cornell Aeronautical Lab. Buffalo, New York	BUORD & BUAER
Curtiss-Wright Corp. Columbus, Ohio Attn: Mr. Bruce Eaton	Bureau of Aeronautics Rep. Curtiss-Wright Corporation Columbus 16, Ohio	BUAER & BUORD
Douglas Aircraft Co. El Segundo Branch El Segundo, California Attn: Mr. E. H. Heinemann	Bureau of Aeronautics Rep. Douglas Aircraft Co. El Segundo, California	BUAER
Douglas Aircraft Co. 3000 Ocean Park Boulevard Santa Monica, California Attn: Mr. A. E. Raymond (1) Mr. E. F. Burton (1)		AAF ORD DEPT
Eastman Kodak Co. Navy Ordnance Division Rochester, New York Attn: Dr. Herbert Trotter	Naval Inspector of Ordnance Navy Ordnance Division Eastman Kodak Co. 50 West Main Street Rochester 4, New York	BUORD
Fairchild Engine & Airplane Corp. NEPA Division P.O. Box 415 Oak Ridge, Tenn. Attn: Mr. A. Kalitinsky, Chief Engineer		AAF
Fairchild Engine & Airplane Corp. Pilotless Plane Division Farmingdale, Long Island, N.Y. Attn: Mr. J. A. Slonim	Representative-in-Charge Fairchild Engine & Airplane Corp. Pilotless Plane Division Farmingdale, Long Island, N.Y.	BUAER
The Franklin Institute Laboratories for Research and Development Philadelphia, Pa. Attn: Mr. R. H. McClarren	Commanding Officer Naval Aircraft Modification Unit Johnsville, Pennsylvania	BUAER
General Electric Co. Project Hermes Schenectady, New York Attn: Mr. C. K. Bauer		ORD DEPT
General Electric Co. Federal & Marine Commercial Division Schenectady, New York Attn: Mr. A. L. Ruiz	Development Contract Officer General Electric Co. Schenectady, New York	BUORD
General Electric Co. Aviation Division Schenectady, New York Attn: Mr. S. A. Schuler, Jr. Mr. Phillip Clasa		AAF

C. PRIME CONTRACTORS (Cont'd)

CONTRACTOR	TRANSMITTED VIA	COGNIZANT AGENCY
Glenn L. Martin Co. Baltimore, Maryland Attn: Mr. N. M. Voorhies	Bureau of Aeronautics Rep. Glenn L. Martin Co. Baltimore, 3, Maryland	BUAER
Glenn L. Martin Company Baltimore 3, Maryland Attn: Mr. W. B. Bergen		AAF
Globe Corp. Aircraft Division Joliet, Illinois Attn: Mr. J. A. Weagle	Inspector of Naval Material 141 W. Jackson Blvd. Chicago 4, Illinois	BUAER
Goodyear Aircraft Corp. Akron, Ohio Attn: Dr. Carl Arnstein	Bureau of Aeronautics Rep. 1210 Massillon Road Akron 15, Ohio	BUAER
Goodyear Aircraft Plant "B" Akron 17, Ohio Attn: Mr. A. J. Peterson		AAF
Grumman Aircraft Engineering Corp. Bethpage, Long Island, N.Y. Attn: Mr. William T. Schwendler	Bureau of Aeronautics Rep. Grumman Aircraft Engr. Corp. Bethpage, L.I., N.Y.	BUAER
Hughes Aircraft Co. Culver City, California Attn: Mr. D. H. Evans		AAF
Jet Propulsion Laboratory California Institute of Technology (2 copies)	Officer-in-Charge Ordnance Research & Development Division Sub-office (Rocket) California Institute of Technology Pasadena 4, California	ORD DEPT
Kellex Corp. New York, New York	Inspector of Naval Material 90 Church Street New York 7, N.Y.	BUORD
M. W. Kellogg Co. Foot of Danforth Avenue Jersey City 3, N.J. Dr. G. H. Messerly		AAF BUORD
Chairman, MIT, GMC (2 copies) Project Meteor Office Massachusetts Institute of Technology Cambridge, Mass. Attn: Dr. H. G. Stever	Navy Ordnance Resident Technical Liaison Officer Massachusetts Institute of Technology Room 20-C-135 Cambridge 39, Mass.	BUORD & AAF
McDonnell Aircraft Corp. St. Louis, Missouri Attn: Mr. W. P. Montgomery	Bureau of Aeronautics Rep. McDonnell Aircraft Corp. P.O. Box 516 St. Louis 21, Missouri	AAF & BUAER
North American Aviation Inc. Los Angeles, California Attn: Dr. Wm. Bollay	Bureau of Aeronautics Resident Representative Municipal Airport Los Angeles 45, Calif.	AAF BUORD & BUAER
Northrop Aircraft Inc. Hawthorne, California		AAF
Princeton University Physics Department Princeton, New Jersey Attn: Dr. John A. Wheeler	Development Contract Officer Princeton University Princeton, New Jersey	BUORD

C. PRIME CONTRACTORS (Cont'd)

CONTRACTOR	TRANSMITTED VIA	COGNIZANT AGENCY
Princeton University (3 copies) Princeton, New Jersey Attn: Project SQUID	Commanding Officer Branch Office Office of Naval Research 90 Church Street - Rm 1116 New York 7, New York	BUAER
Radio Corporation of America Victor Division Camden, New Jersey Attn: Mr. T. T. Eaton		AAF & BUORD
Radioplane Corporation Metropolitan Airport Van Nuys, California	Bureau of Aeronautics Rep. Lockheed Aircraft Corp. 2555 North Hollywood Way Burbank, California	BUAER
Raytheon Manufacturing Co. Waltham, Massachusetts Attn: Mrs. H. L. Thomas	Inspector of Naval Material Park Square Building Boston 16, Mass.	AAF & BUAER
Reeves Instrument Corp. 215 E. 91st Street New York 28, N.Y.	Inspector of Naval Material 90 Church St. New York 7, N.Y.	BUAER
Republic Aviation Corp. Military Contract Dept. Farmingdale, L.I., N.Y. Attn: Dr. William O'Donnell		AAF
Ryan Aeronautical Co. Lindberg Field San Diego 12, California Attn: Mr. B. T. Salmon		AAF
S. W. Marshall Co. Shoreham Building Washington, D. C.	Inspector of Naval Material 401 Water Street Baltimore 2, Maryland	BUAER
Sperry Gyroscope Co., Inc. Great Neck, L.I., N.Y.	Inspector of Naval Material 90 Church Street New York 7, N.Y.	BUAER ORD DEPT
United Aircraft Corp. Chance Vought Aircraft Div. Stratford, Conn. Attn: Mr. P. S. Baker	Bureau of Aeronautics Rep. United Aircraft Corp. Chance Vought Aircraft Div. Stratford 1, Conn.	BUAER
United Aircraft Corp. Research Department East Hartford, Conn. Attn: Mr. John G. Lee	Bureau of Aeronautics Rep. United Aircraft Corp. Pratt & Whitney Aircraft Div. East Hartford 8, Conn.	BUORD
University of Michigan Aeronautical Research Center Willow Run Airport Ypsilanti, Michigan Attn: Mr. R. F. May Dr. A. M. Kuethe		AAF
University of Southern California Naval Research Project, College of Engineering Los Angeles, California Attn: Dr. R. T. DeVault	Bureau of Aeronautics Rep. 15 South Raymond Street Pasadena, California	BUAER
University of Texas Defense Research Lab. Austin, Texas Attn: Dr. C. P. Boner	Development Contract Officer 500 East 24th Street Austin 12, Texas	BUORD
Willys-Overland Motors, Inc. Maywood, California Attn: Mr. Joe Talley	Representative-in-Charge, BUAER Consolidated-Vultee Aircraft Corp. Downey, California	BUAER

D. COMPONENT CONTRACTORS

(1) AERODYNAMICS & BALLISTICS

CONTRACTOR	TRANSMITTED VIA	COGNIZANT AGENCY
New Mexico School of Mines Research & Development Div. Albuquerque, New Mexico	Development Contract Officer New Mexico School of Mines Albuquerque, New Mexico	BUORD
New Mexico School of Agriculture & Mechanic Arts State College, New Mexico Attn: Dr. George Gardner	Development Contract Officer New Mexico School of Mines Albuquerque, New Mexico	BUORD
New York University Applied Mathematics Center New York, New York Attn: Mr. Richard Courant	Inspector of Naval Material 90 Church Street New York 7, New York	BUAER
Office of the Chief of Ordnance Ordnance Research & Development Division Research & Materials Branch Ballistics Section Pentagon Washington 25, D.C.		ORD DEPT
Polytechnic Institute of Brooklyn Brooklyn, New York Attn: Mr. R.P. Harrington	Inspector of Naval Material 90 Church Street New York 7, New York	BUAER
University of Minnesota Minneapolis, Minnesota Attn: Dr. Akerman	Inspector of Naval Material Federal Bldg. Milwaukee 2, Wis.	BUORD
Aerojet Engineering Corp. Azusa, California Attn: K.F. Mundt	Bureau of Aeronautics Rep. 15 South Raymond Street Pasadena, California	BUAER
Marquardt Aircraft Co. Venice, California Attn: Dr. R. E. Marquardt	Bureau of Aeronautics Rep. 15 South Raymond Street Pasadena, California	BUAER

(2) GUIDANCE & CONTROL

Belmont Radio Corporation 5921 West Dickens Avenue Chicago 29, Illinois Attn: Mr. Harold C. Mattes		AAF
Bendix Aviation Corp. Eclipse-Pioneer Division Teterboro, New Jersey Attn: Mr. R. C. Sylvander	Bureau of Aeronautics Resident Representative Bendix Aviation Corp. Teterboro, New Jersey	BUAER
Bendix Aviation Corp. Pacific Division, SPD West North Hollywood, Calif.	Development Contract Officer Bendix Aviation Corp. 11600 Sherman Way North Hollywood, California	BUORD
Bendix Aviation Radio Division East Joppa Road Baltimore 4, Maryland Attn: Mr. J. W. Hammond		AAF
Buehler and Company 1607 Howard Street Chicago 26, Illinois Attn: Mr. Jack M. Roehn		AAF
Commanding General Army Air Forces Pentagon Washington 25, D.C. Attn: AC/AS-4, DRE-2F		AAF

D. COMPONENT CONTRACTORS (Cont'd)

(2) GUIDANCE & CONTROL

CONTRACTOR	TRANSMITTED VIA	COGNIZANT AGENCY
Consolidated-Vultee Aircraft Corporation San Diego, California Attn: Mr. C. J. Breitwieser	Bureau of Aeronautics Representative, Consolidated-Vultee Aircraft Corp. San Diego, California	BUAER
Cornell University Ithaca, New York Attn: Mr. William C. Ballard, Jr.		AAF
Director, U.S. Navy Electronics Laboratory, San Diego, California		NAVY
Electro-Mechanical Research Ridge Field, Connecticut Attn: Mr. Charles B. Aiken		AAF
Farnsworth Television and Radio Co. Fort Wayne, Indiana Attn: Mr. J. D. Schantz	DCO, Applied Physics Laboratory Johns Hopkins University 8621 Georgia Avenue, Silver Spring, Maryland	BUORD
Federal Telephone and Radio Corp. 200 Mt. Pleasant Avenue Newark 4, New Jersey Attn: Mr. E. N. Wendell		AAF
Galvin Manufacturing Corp. 4545 Augusta Blvd. Chicago 5, Illinois Attn: Mr. G. R. MacDonald		AAF
G. M. Giannini and Co., Inc. 285 West Colorado St. Pasadena, California	Bureau of Aeronautics Rep. 15 South Raymond St. Pasadena, California	BUAER
Gilfillan Corp. 1815-1849 Venice Blvd. Los Angeles 6, California Attn: Mr. G. H. Miles		AAF
Hillyer Engineering Co. New York, New York Attn: Mr. Curtiss Hillyer	Inspector of Naval Material 90 Church Street New York 7, New York	BUAER
Kearfott Engineering Co. New York, New York Attn: Mr. W. A. Reichel	Inspector of Naval Material 90 Church Street New York 7, New York	BUAER
Lear Incorporated 110 Iona Avenue, N.W. Grand Rapids 2, Michigan Attn: Mr. R.M. Mock		AAF
Manufacturers Machine & Tool Co. 320 Washington Street Mt. Vernon, N.Y. Attn: Mr. L. Kenneth Mayer, Comptroller		AAF
Minneapolis-Honeywell Mfgr. Co. 2753 Fourth Avenue Minneapolis 8, Minnesota Attn: Mr. W. J. McGoldrick, Vice-President		AAF
Ohio State University Research Foundation Columbus, Ohio Attn: Mr. Thomas E. Davis, Staff Assistant		AAF

D. COMPONENT CONTRACTORS (Cont'd)

(2) GUIDANCE & CONTROL

CONTRACTOR	TRANSMITTED VIA	COGNIZANT AGENCY
Haller, Raymond & Brown P.O. Box 342 State College, Pennsylvania Attn: Dr. R. C. Raymond, Pres.		AAF
Office of Chief Signal Officer Engineering & Technical Services, Engineering Division Pentagon Washington 25, D.C.		ORD DEPT
Raytron, Inc. 209 E. Washington Avenue Jackson, Michigan Attn: Mr. John R. Gelzer, Vice-Pres.		AAF
L. N. Schwein Engineering Co. 5736 Washington Blvd. Los Angeles 16, California Attn: L.N. Schwein, General Partner		AAF
Senior Naval Liaison Officer U.S. Naval Electronic Liaison Office Signal Corps, Engineering Laboratory Fort Monmouth, New Jersey		NAVY
Servo Corporation of America Huntington, L.I., New York	Inspector of Naval Material 90 Church Street New York 7, New York	BUAER
Square D Co. Kollsman Instrument Division Elmhurst, New York Attn: Mr. V. E. Carbonara	Bureau of Aeronautics Rep. 90 Church Street New York 7, New York	BUAER
Stromberg-Carlson Company Rochester, New York Attn: Mr. L.L. Spencer, Vice-Pres.		AAF
Submarine Signal Company Boston, Massachusetts Attn: Mr. Edgar Horton	Development Contract Officer Massachusetts Institute of Technology Cambridge 39, Massachusetts	BUORD
Summers Gyroscope Co. 1100 Colorado Avenue Santa Monica, California Attn: Mr. Tom Summers, Jr.		AAF
Sylvania Electric Products Inc. Flushing, Long Island, N.Y. Attn: Dr. Robert Bowie	Inspector of Naval Material 90 Church Street New York 7, New York	BUORD
University of Illinois Urbana, Illinois Attn: Mr. H. E. Cunningham, Sec.		AAF
University of Pennsylvania Moore School of Electrical Engr. Philadelphia, Pa.	Commanding Officer Naval Aircraft Modification Unit Johnsville, Pa.	BUAER
University of Pittsburgh Pittaburgh, Pennsylvania Attn: Mr. E. A. Holbrook, Dean		AAF
University of Virginia Phyaics Department Charlottesville, Virginia Attn: Dr. J. W. Beams	Development Contract Officer University of Virginia Charlottesville, Virginia	BUORD

D. COMPONENT CONTRACTORS (Cont'd)

(2) GUIDANCE & CONTROL

CONTRACTOR	TRANSMITTED VIA	COGNIZANT AGENCY
Washington University Research Foundation 8135 Forsythe Blvd., Clayton 5, Missouri Attn: Dr. R. G. Spencer		AAF
Westinghouse Electric Corp. Springfield, Massachusetts Attn: J.K.B. Hare, Vice-Pres. (Dayton Office)		AAF
Director of Specialty Products Development Whippany Radio Laboratory Whippany, N.J. Attn: Mr. M.H. Cook		ORD DEPT
Zenith Radio Corporation Chicago, Illinois Attn: Hugh Robertson, Executive Vice-Pres.		AAF

(3) PROPULSION

Aerojet Engineering Corp. Azusa, California Attn: K.F. Mundt	Bureau of Aeronautics Rep. 15 South Raymond Street Pasadena, California	BUAER
Armour Research Foundation Technical Center, Chicago 16, Illinois Attn: Mr. W. A. Casler		ORD DEPT
Arthur D. Little, Inc. 30 Memorial Drive, Cambridge, Mass. Attn: Mr. Helge Holst		ORD DEPT
Battelle Memorial Institute 505 King Avenue Columbus 1, Ohio Attn: Dr. B. D. Thomas		AAF & BUAER
Bendix Aviation Corp. Pacific Division, SPD West N. Hollywood, Calif.	Development Contract Officer Bendix Aviation Corp. 11600 Sherman Way N. Hollywood, Calif.	BUORD
Bendix Products Division Bendix Aviation Corporation 401 Bendix Drive South Bend 20, Indiana Attn: Mr. Frank C. Mock		AAF BUORD
Commanding General Army Air Forces Pentagon Washington 25, D.C. Attn: AC/AS-4 DRE-2E		AAF
Commanding General Air Materiel Command Wright Field Dayton, Ohio Attn: TSEPP-4B(2) TSEPP-4A(1) TSEPP-5A(1) TSEPP-5C(1) TSORE-(1)		
Commanding Officer Picatinny Arsenal Dover, New Jersey Attn: Technical Division		ORD DEPT

D. COMPONENT CONTRACTORS (Cont'd)

(3) PROPULSION

CONTRACTOR	TRANSMITTED VIA	COGNIZANT AGENCY
Commanding Officer Watertown Arsenal Watertown 72, Massachusetts. Attn: Laboratory.		ORD DEPT
Continental Aviation and Engr. Corp. Detroit, Michigan	Bureau of Aeronautics Rep. 11111 French Road Detroit 5, Michigan	BUAER & AAF
Curtiss-Wright Corporation Propeller Division Caldwell, New Jersey Attn: Mr. C. W. Chillson		AAF
Experiment, Incorporated Richmond, Virginia Attn: Dr. J. W. Mullen, II	Development Contract Officer P.O. Box 1-T Richmond 2, Virginia	BUORD
Fairchild Airplane & Engine Co. Ranger Aircraft Engines-Div. Farmingdale, L.I., New York	Bureau of Aeronautics Rep. Bethpage, L.I., N.Y.	BUAER
General Motors Corporation Allison Division Indianapolis, Indiana Attn: Mr. Ronald Hazen	Bureau of Aeronautics Rep. General Motors Corporation Allison Division Indianapolis, Indiana	BUAER
G. M. Giannini & Co., Inc. 285 W. Colorado St. Pasadena, California		AAF
Hercules Powder Co. Port Ewen, N.Y.	Inspector of Naval Material 90 Church Street New York 7, New York	BUORD
Marquardt Aircraft Company Venice, California Attn: Dr. R. E. Marquardt	Bureau of Aeronautics Rep. 15 South Raymond Street Pasadena, California	AAF BUAER
Menasco Manufacturing Co. 805 E. San Fernando Blvd. Burbank, California Attn: Robert R. Miller Exec. Vice-Pres.		AAF
New York University Applied Mathematics Center New York, New York Attn: Dr. Richard Courant	Inspector of Naval Material 90 Church Street New York 7, New York	BUAER
Office of Chief of Ordnance Ordnance Research & Development Div. Rocket Branch Pentagon, Washington 25, D.C.		ORD DEPT
Polytechnic Institute of Brooklyn Brooklyn, New York Attn: Mr. R.P. Harrington	Inspector of Naval Material 90 Church Street New York 7, New York	BUAER
Purdue University Lafayette, Indiana Attn: Mr. G. S. Meikel	Inspector of Naval Material 141 W. Jackson Blvd. Chicago 4, Illinois	
Reaction Motors, Inc. Lake Denmark Dover, New Jersey	Bureau of Aeronautics Resident Representative Reaction Motors, Inc. Naval Ammunition Depot Lake Denmark, Dover, N.J.	BUAER

D. COMPONENT CONTRACTORS (Cont'd)

(3) PROPULSION

CONTRACTOR	TRANSMITTED VIA	COGNIZANT AGENCY
Rensselaer Polytechnic Institute Troy, New York Attn: Instructor of Naval Science		BUORD
Solar Aircraft Company San Diego 12, California Attn: Dr. M.A. Williamson		ORD DEPT
Standard Oil Company Esso Laboratories Elizabeth, New Jersey	Development Contract Officer Standard Oil Company Esso Laboratories, Box 243 Elizabeth, New Jersey	BUORD
University of Virginia Physics Department Charlottesville, Virginia Attn: Dr. J. W. Beams	Development Contract Officer University of Virginia Charlottesville, Virginia	BUORD
University of Wisconsin Madison, Wisconsin Attn: Dr. J.O. Hirschfelder	Inspector of Naval Material, 141 W. Jackson Blvd. Chicago 4, Illinois	BUORD
Westinghouse Electric Co. Essington, Pennsylvania	Bureau of Aeronautics Resident Representative Westinghouse Electric Corp. Essington, Pennsylvania	BUAER
Wright Aeronautical Corp. Woodridge, New Jersey	Bureau of Aeronautics Rep. Wright Aeronautical Corp. Woodridge, New Jersey	BUAER
Bethlehem Steel Corp. Shipbuilding Division Quincy 69, Mass. Attn: Mr. B. Fox	Supervisor of Shipbuilding, USN Quincy, Mass.	BUAER